Research Square

Preprints are preliminary reports that have not undergone peer review.
They should not be considered conclusive, used to inform clinical practice,
or referenced by the media as validated information.

A Performance-Based Classification Framework for Standardising FA/GGBFS Geopolymer Binder Systems

Ibrahim Alameri

i.ameri@su.edu.ye

Sana'a University

Salam R. Armoosh

University of Anbar

F. E. Hanash

Sa'dah University

Systematic Review

Keywords: Supplementary Cementitious Materials (SCMs), Performance Classification, Standardisation, Mechanical & Durability Performance, Low-Clinker Sustainable Binders

Posted Date: June 12th, 2026

DOI: https://doi.org/10.21203/rs.3.rs-9784602/v1

License: This work is licensed under a Creative Commons Attribution 4.0 International License. Read Full License

Additional Declarations: No competing interests reported.

Version of Record: A version of this preprint was published at Discover Materials on August 24th, 2026. See the published version at https://doi.org/10.1007/s43939-026-00929-4.

Abstract

The necessity of reducing CO_2 emissions resulting from cement production has increased the demand for supplementary cementitious materials (SCMs), such as fly ash (FA) and ground granulated blast furnace slag (GGBFS). However, the widespread adoption of these materials has remained limited due to variability in quality, inconsistency in supply, and a lack of standardized performance specifications. Alkali-activated geopolymer binders derived from FA and GGBFS have shown mechanical performance and durability superior to, ordinary Portland cement (OPC). This behaviour is attributed to the formation of two gel phases (N A S H and C (A) S H) depending on the calcium content of the raw material. However, no standardized classification or performance-based design framework was established for these materials within current codes and regulations. In accordance with the PRISMA 2020 guidelines, a systematic review of published literature (2010–2025) was conducted. Four key factors governing 28-day compressive strength were identified: FA/GGBFS ratio, NaOH molarity (8–14 M), SS/SH ratio (1.5–2.5), and water to binder ratio (0.35–0.45). Quantitative relationships were established between mix design variables and engineering performance. Under ambient curing conditions, binary geopolymer concrete composed of FA/GGBFS achieved compressive strengths ranging from 45 to 85 MPa. Based on these results, a five-tier performance classification framework (GPC I to GPC V) was proposed. This framework correlates the chemical composition of the raw materials, the predominant gel type, the strength class, and the durability class (DC 1 to DC 5). This framework was expanded to provide preliminary guidelines for mix design and performance classification. The results demonstrated the potential to integrate FA/GGBFS geopolymers into broader standardization strategies for the construction materials.

1. Introduction

Concrete is the most widely used construction material globally, with annual production exceeding 10 billion tonnes and continuing to increase due to rapid urbanization and infrastructure demand (Afsoosbiria & Machowska, 2025; Al Khaffaf et al., 2025; Meyer, 2009). Its primary binder, ordinary Portland cement (OPC), is highly carbon-intensive, as clinker production involves the calcination of limestone, releasing significant amounts of CO_2, and contributing approximately 7–8% of total global anthropogenic CO_2 emissions (Al Khaffaf et al., 2025; Van Roijen et al., 2024). Given that the construction and buildings sector accounts for roughly one-third of global CO_2 emissions, cement production represents a critical target for industrial decarbonization (Cheng et al., 2023).

This urgency is further underscored by atmospheric CO_2 concentrations to levels (~ 417–420 ppm), the highest level seen in at least 2.5 million years (Da et al., 2019; Hönisch et al., 2023; IPCC, 2023; Rae et al., 2021), highlighting the need for low-carbon alternatives in the built environment to mitigate ongoing climate change (Berends et al., 2021; Pearson & Palmer, 2000).

Geopolymer concrete has attracted sustained research interest as a low-carbon structural binder (Almutairi et al., 2021; Amran et al., 2020; Farooq et al., 2021; Provis, 2018). Geopolymers are inorganic polymers formed through the alkaline activation of aluminosilicate-rich industrial by-products, most commonly FA and GGBFS, without high-temperature combustion(Davidovits, 1991; Provis et al., 2015). Davidovits established the intellectual foundations for modern geopolymer science in the late 1970s, demonstrating that the polycondensation of calcined aluminosilicates in an alkaline medium yields a three-dimensional network with properties well-suited to structural applications (Davidovits, 1991, 2008). The geopolymerization reaction occurs

through the alkaline dissolution of aluminosilicate species, the migration of dissolved monomers, and the polycondensation into a rigid cross-linked network, a mechanism that is fundamentally different from the calcium silicate hydrate (C-S-H) formation in the hydration of Portland cement (Duxson et al., 2007; Provis et al., 2015)

FA and GGBFS are considered the most technically and commercially viable raw materials for the production of high-quality GPC (Hu et al., 2019; R. P. Singh et al., 2023). Both are produced as industrial by-products in enormous quantities. Global production of FA is estimated at between 800 and 1,000 million tons per year, with utilization rates not exceeding 45–50% (Ahmaruzzaman, 2010; Blissett & Rowson, 2012; Yao et al., 2015), while production of GGBFS exceeds 300 million tons per year (Aïtcin, 2000; Giergiczny, 2019; Meyer, 2009). Their use as binding components allows for a direct replacement of OPC, thus avoiding the burden of landfill waste resulting from current disposal practices, as well as the energy-intensive clinker combustion that is the basis of OPC manufacturing (Almutairi et al., 2021; Amran et al., 2020). Life cycle assessments (LCA) consistently show a reduction in CO_2 emissions of 35–80% compared to OPC concrete when using FA and GGBFS as precursor materials (Passuello et al., 2017; Turner & Collins, 2013).

The mechanical properties of FA/GGBFS GPC are now well established. Binary systems achieve compressive strengths of 50–85 MPa after 28-day ambient curing, meeting standard- to high-strength structural requirements (Mehta et al., 2020). GPC exhibits no expansive degradation under sulphate attack, low chloride diffusion, and retains more than 90% of its compressive strength after fire exposure at 800°C, performance categories in which it consistently outperforms OPC concrete (Alahmari et al., 2023; Taher et al., 2024; Wong, 2022).

Despite these advantages, structural adoption continues to be constrained by the lack of consistent design standards, the variability of raw materials, the environmental burden of alkali activators, and the limited availability of long-term field data (Nodehi & Taghvaee, 2022; Tahwia et al., 2024). This review addresses these challenges by following the PRISMA 2020 guidelines (Page et al., 2021) and applying clear inclusion/exclusion criteria. Furthermore, it proposes a unique GPC performance classification matrix as a practical tool for structural specification, and offers a critical assessment of the inconsistencies and reliability issues within the synthesized dataset, thereby providing contributions not addressed in previous reviews (Almutairi et al., 2021; Farooq et al., 2021; Scrivener et al., 2018).

2. Methodology

2.1 Search Strategy and Database Selection

This review covers FA/GGBFS based geopolymer concretes, focusing specifically on binary and ternary precursor systems suitable for structural applications. In February 2025, a systematic literature search was conducted using two major academic databases (Scopus and Web of Science) in accordance with the PRISMA 2020 reporting guidelines (Page et al., 2021). The search string applied was: (*“geopolymer concrete” OR “alkali-activated concrete” OR “alkali-activated binder”*) AND (*“fly ash” OR “GGBFS” OR “slag”*) AND (*“compressive strength” OR “durability” OR “life cycle assessment” OR “carbonation” OR “chloride”*). The search was restricted to articles published in scientific journals and conference proceedings in English between January 2010 and February 2025. Unpublished literature, academic theses, and nonpeer-reviewed reports were excluded. The initial

database search yielded 1,423 records. After the automatic removal of duplicate records, 1,021 unique records were identified, and the search then proceeded to the title and abstract screening phase.

2.2 Study Selection Criteria

Studies providing quantitative data on the mechanical properties or durability of FA/GGBFS-based GPC were included, provided they featured clear documentation of mix design parameters (FA/GGBFS ratio, NaOH molarity, SS/SH ratio, w/b ratio, and curing conditions). Studies presenting only qualitative results without quantitative data, utilizing precursor systems falling outside the scope of binary or ternary FA/GGBFS mixtures (e.g., metakaolin-only systems), or lacking reproducible documentation of the mix design were excluded.

Following the screening of titles and abstracts, 843 records were excluded, leaving 178 publications for full-text assessment. Of these, 73 studies met all inclusion criteria and were retained as primary data sources. Additionally, 22 supplementary references, including foundational texts and key review papers providing essential contextual background, were added through citation searching within the key review papers. Consequently, the final reference dataset comprises 95 cited publications. Table 1 summarizes the entire study selection process.

Table 1
Study selection summary.

Stage	Records / Outcome
Records identified (Scopus)	847
Records identified (Web of Science (Core Collection))	576
Records after deduplication	1,021
Records excluded at title/abstract screening	843
Full-text articles assessed for eligibility	178
Primary studies meeting all inclusion criteria	73
Background/context references added via citation snowballing	22
Total references cited in this review	95
Date range of included studies	January 2010 – February 2025
Key databases searched	Scopus; Web of Science (Core Collection)
Search date	February 2025

2.3 Data Extraction and Quality Assessment

In this study, the data quality was assessed according to three criteria, including statistical reporting expressed as mean ± standard deviation or range, adequate sample size with a minimum of three replicates per mix, and evidence of independent laboratory replication. Studies meeting all three criteria were classified as high confidence; those meeting two as medium confidence; and one or fewer as low confidence. Of the 73 primary studies meeting the inclusion criteria, 34 were classified as high confidence, 29 as medium confidence, and 10 as low confidence. Only the 63 high- and medium-confidence studies were used for statistical synthesis of

compressive strength and durability data; low-confidence studies were retained for qualitative discussion only. Contradictions between studies were identified by cross-tabulation of extracted data and explained mechanistically where sufficient microstructural evidence existed.

3. Geopolymerization Chemistry and Microstructure

Geopolymerization is a heterogeneous, exothermic polycondensation reaction in which amorphous aluminosilicate phases dissolve under strongly alkaline conditions and reorganise into a three-dimensional cross-linked inorganic polymer network (Duxson et al., 2007; Freire et al., 2022; Matsimbe et al., 2022; Provis et al., 2015; J. Singh & Singh, 2019). The reaction was first systematically described by Davidovits, 1991, who established that the polycondensation of aluminosilicate monomers in alkaline medium proceeds through nucleophilic substitution and condensation reactions, ultimately yielding a rigid, X-ray-amorphous framework. Subsequent mechanistic work has confirmed and extended this model across a wide range of precursor chemistries (Fernández-Jiménez & Palomo, 2005; Xu & Van Deventer, 2000)

The reaction occurs through three overlapping stages (El Fadili et al., 2025). First, aluminosilicate phases dissolve from precursor particle surfaces at pH above 14, releasing $Si(OH)_4$ and $Al(OH)_4^-$ monomers into solution (El Fadili et al., 2025; Marvila et al., 2021). This stage strongly depends on the concentration of the activator and the reactive glass content of the raw material (Adewuyi, 2021; Kolade et al., 2025; Sindhunata et al., 2006).

In the next step, these species migrate and condense through nucleophilic attack and the elimination of water expulsion to form oligomeric intermediate gels. Finally, the developing gel network hardens through ongoing polycondensation to form a three-dimensional rigid structure (Duxson et al., 2007; Palomo et al., 1999). Figure 1 illustrates the reaction sequence and its relationship with compressive strength, expressed in terms of GGBFS content and Si/Al molar ratio. In mixes rich of FA, a low calcium content means that the dissolution of the glassy aluminosilicate phase is the rate-limiting step. This requiring high curing temperatures (60–80°C for 24 hours) to attain adequate strength at the early stages. The incorporation of GGBFS significantly accelerates the reaction by providing active calcium species that initiate the rapid formation of C-A-S-H, thereby lowering the energy barrier for network formation and enabling the development of concrete strength at ambient temperature (Luo et al., 2022; Naresh et al., 2026; Puligilla & Mondal, 2013; Wang et al., 2026; Xiao et al., 2024).

The nature of the predominant reaction product formed depends on the calcium content of the precursor substance. Low-calcium Class F fly ash systems produce a sodium aluminosilicate hydrate (N-A-S-H) gel which consists of a three-dimensional tetrahedral framework stabilized by sodium ions. This gel structure is responsible for the notable thermal stability and chemical resistance of geopolymer concrete (Degefu & Berardi, 2024; Duxson et al., 2007; Wan et al., 2020). High-calcium precursors such as GGBFS shift the reaction product toward calcium aluminosilicate hydrate (C-A-S-H), structurally analogous to OPC hydration products but with a distinct Al/Si ratio and pore chemistry (Kolade et al., 2025; Zhang et al., 2020)). Binary FA/GGBFS systems generate a co-existing N-A-S-H/C-A-S-H hybrid matrix. (Puligilla & Mondal, 2013) demonstrated using SEM-EDS and semi-adiabatic calorimetry that C-A-S-H precipitation is initiated first upon contact of GGBFS with the alkaline solution, and that this early C-A-S-H formation subsequently accelerates the geopolymerization of fly ash, yielding a denser and more homogeneous final matrix than either precursor achieves individually. (Bernal et al., 2013) further characterised this hybrid gel using X-ray pair distribution function analysis, confirming that the

N-A-S-H and C-A-S-H phases co-exist at the nanoscale and that the degree of intermixing controls both carbonation susceptibility and long-term mechanical stability. This hybrid architecture, combining the rapid strength gain of C-A-S-H with the long-term chemical durability of N-A-S-H, has emerged as the optimal microstructural configuration for ambient-cured structural GPC (Bernal et al., 2013). Formation of the hybrid gel has been confirmed by solid-state ^{29}Si and ^{27}Al magic angle spinning nuclear magnetic resonance (MAS-NMR) spectroscopy across multiple independent laboratories. (Duxson et al., 2007) demonstrated that ^{29}Si MAS-NMR resolves the $Q^4(mAl)$ silicon environments characteristic of the N-A-S-H network, providing unambiguous evidence of the cross-linked tetrahedral framework. (Myers et al., 2013) extended this approach with a generalised structural model for C-A-S-H/N-A-S-H co-existing gels, demonstrating that the cross-linked substituted tobermorite model accurately describes the calcium-rich phase in blended FA/GGBFS systems and confirming that both gel types must be accounted for in service-life models.

As shown in Fig. 1(b), the molar ratio of Si/Al in the final network is a critical design variable: while values between 1.5 and 2.5 are associated with optimum compressive strength and high chemical resistance, exceeding this range either reduces cross-linking density (Si/Al < 1.5, promotes zeolite crystallization) or yields silica-rich gels characterized by weak cross-linking (Si/Al > 2.5) and poor mechanical performance (Duxson et al., 2007). Typically, an alkaline activator, specifically NaOH, combined with a sodium silicate (Na_2SiO_3) solution provides the high-pH environment necessary for rapid dissolution and supplies additional reactive silica to adjust the Si/Al ratio. Consequently, the mass ratio of Na_2SiO_3 to NaOH (SS/SH) stands as one of the most sensitive mixing design parameters, as it profoundly influences gel formation kinetics, microstructure density, and ultimate mechanical performance (Fernández-Jiménez & Palomo, 2005; Kolade et al., 2025).

Curing temperature provides additional control over geopolymerization kinetics. Class F fly ash-dominant systems require elevated curing (60–80°C, 24 h) to overcome the energy barrier to glassy-phase dissolution. (Sindhunata et al., 2006) demonstrated that increasing curing temperature from 35°C to 75°C increased the degree of reaction of Class F fly ash from approximately 30% to over 70% at equivalent activator concentrations. The addition of slag significantly reduces this barrier by providing reactive calcium which accelerates dissolution kinetics, enabling the development of ambient temperature strength in binary FA/GGBFS systems at slag contents above 30%, a result that has been consistently reported across independent experiments (Hussein & Fawzi, 2021; Nath & Sarker, 2014; Samantasinghar & Singh, 2019; Zhao et al., 2024), as reflected in the strength trends shown in Fig. 1(a).

4. Precursor and Activator Materials

4.1 Aluminosilicate Precursors

The oxide chemistry of the raw material is the fundamental determinant of geopolymer network formation, gel type, and long-term performance. Based on experimental characterization data, Table 2 summarizes the validated oxide composition ranges for the primary precursors utilized in structural GPC. These compositional data exhibit significant and practical variability whose chemistry depends on the coal source, the combustion technology employed, and the collection efficiency of the electrostatic precipitators. This source-specific variability remains a significant challenge in the transfer of laboratory-optimized mix designs to field applications (Emarah, 2025; Kolade et al., 2025).

Table 2
Typical oxide composition ranges of principal precursor materials used

Precursor	SiO_2 (wt%)	Al_2O_3 (wt%)	CaO (wt%)	Fe_2O_3 (wt%)	MgO (wt%)	LOI (wt%)	References
Class F Fly Ash	45–60	20–35	1–8	4–15	0.5–2.0	0.5–4.0	(Deb et al., 2014; Nath & Sarker, 2014; Zhang et al., 2020)
Class C Fly Ash	34–44	18–26	20–30	5–10	3–8	0.5–2.0	(Puertas et al., 2000; Zhang et al., 2020)
GGBFS	32–38	10–15	36–44	0.2–1.5	5–12	< 2	(Deb et al., 2014; Nath & Sarker, 2014)
Metakaolin	50–55	40–45	< 2	< 2	< 1	< 1	(Aslan & Erkan, 2024)
Mine Tailings (ilmenite)	45–55	10–18	5–12	10–20	3–8	1–3	(Brekke & O'Born, 2025)

Class F fly ash is considered the most extensively studied precursor material for the production of geopolymers (GPC). Its low CaO content (1–8% by weight) promotes the formation of a thermally and chemically resistant N-A-S-H gel, thereby accounting for the superior acid and fire resistance exhibited by geopolymers (Zhang et al., 2020). Its main limitations, however, include a reliance on thermal curing (given that the dissolution of the glassy phase in pure FA mixes is kinetically limited at room temperature) and significant variability in composition from one source to another, resulting from differences in coal mineralogy and combustion conditions (Emarah, 2025; Kolade et al., 2025).

Class C fly ash contains a significantly higher proportion of CaO (20–30% by weight) and exhibits inherent self-hardening activity that eliminates the reliance on heat curing. However, its high C-A-S-H content reduces sulfate resistance, particularly in FA/GGBFS mixtures, where slag-rich formulations (> 60% GGBFS) already carry some risk of ettringite formation under severe sulfate exposure (Wong, 2022).

GGBFS is considered the most reactive complementary precursor material in binary GPC mixures. Its high CaO content (36–44% by weight) rapidly catalyzes the formation of C-A-S-H upon alkaline activation. This facilitates strength gain in concrete mixtures at room temperature thereby significantly reducing the reliance on heat curing (Puertas et al., 2000). Furthermore, (Deb et al., 2014) confirmed through calorimetry that the heat of reaction in FA/GGBFS mixtures increases proportionally with the GGBFS content, thereby accelerating the setting and early strength development. This thermal contribution must be carefully managed in large-volume GGBFS-rich mixtures. (Samantasinghar & Singh, 2019) identified an optimal FA/GGBFS ratio ranging between 60:40 and 50:50 to ensure adequate workability at room temperature. Exceeding this ratio accelerates the nucleation of C-A-S-H, thereby reducing the working time below practical limits when utilizing an 8 M NaOH solution. (Zhao et al., 2024) reported a steady increase in strength with increasing slag content (up to 70%) when utilizing a 10 M NaOH solution. Thus, the elevated concentration of the activator sufficiently retards the formation rate of C-A-S-H to maintain a workable consistency. This interaction between the FA/GGBFS ratio and NaOH concentration constitutes a critical factor in mix design, one that is consistently overlooked by single-variable studies (Hussein & Fawzi, 2021).

Metakaolin is characterized by its high purity and consistent reactivity, attributes owed to a precisely controlled calcination process conducted at temperatures ranging between 600 and 800°C, which results in the near-complete transformation of the kaolinite structure into an amorphous state. However, this calcination process demands higher energy consumption per ton compared to FA or GGBFS thereby limiting its economic viability as a primary raw material for the large-scale production of structural GPC (Aslan & Erkan, 2024). Conversely, Mine tailings, represent a validated emerging precursor pathway. (Brekke & O'Born, 2025) demonstrated that ilmenite tailings from Norwegian processing operations produced GPC with a compressive strength ranging between 35 and 60 MPa and a reduction in CO2 emissions of 57–65% compared to OPC concrete, while simultaneously utilizing a waste stream that would otherwise have required landfill disposal.

Natural clays and agricultural silica-rich by-products (such as rice husk ash) represent additional precursor for diversifying raw materials of increasing strategic importance, particularly as the European Union's commitments to phase out coal create structural vulnerabilities in the supply of FA (Islam et al., 2025; Qin et al., 2022). (Kumar et al., 2008) demonstrated that mechanical activation achieved through high-energy grinding to a particle size of less than d50 = 10 μm significantly enhances both the specific surface area and the reactive glass content of moderately reactive raw materials. This approach offers a practical pathway for upgrading the quality of marginal-grade raw material batches without the need for chemical pre-treatment. The criteria used to assess the quality of raw materials for GPC (specifically reactive glass content, fineness, and pozzolanicity) are calibrated against the performance standards established for supplementary cementitious materials used in OPC concrete (Lothenbach et al., 2011; Mehta & Siddique, 2017; Neville, 2011).

4.2 Alkaline Activators

NaOH and Na_2SiO_3 are the most frequently used activator components in the literature, and their combined chemical composition controls the Si/Al ratio, setting time, workability, and, ultimately, the compressive strength and durability of the hardened GPC. Figure 2 illustrates the sensitivity of compressive strength to both NaOH molarity and SS/SH ratio.

The molarity of NaOH controls the dissolution kinetics of the glassy phase of aluminosilicates. At concentrations below 8 M, dissolution is incomplete; consequently, particularly in systems rich in FA, where the glassy phase is less reactive than that of GGBFS, early age strength development is insufficient for structural applications (Fernández-Jiménez & Palomo, 2005). At concentrations exceeding 14 M, excess Na^+ ions disrupt the formation of the gel network and and cause white efflorescence deposits on hardened GPC surfaces through surface carbonation of residual sodium hydroxide (Hussein & Fawzi, 2021). As illustrated in Fig. 2(a), NaOH concentrations of 10–12 M represent the optimal range across all the data examined, yielding the highest compressive strength at all levels of granulated blast furnace slag content. The reaction is not homogeneous across all three levels of GGBFS content. After 12 months, strength declines by 8–15% as a result of the disruption of the gel network structure caused by excess sodium (Tahwia et al., 2024).

The SS/SH mass ratio controls the amount of reactive silica available to form the network and is a critical variable in the optimization process. As shown in Fig. 2(b), values between 1.5 and 2.5 consistently maximize compressive strength. The addition of soluble silica raises the Si/Al molar ratio of the resulting gel to the optimal range (1.5–2.5).

When the SS/SH ratio exceeds 2.5, the further addition of silicates leads to a reduction in strength due to the poorly cross-linked gel regions (Aslan & Erkan, 2024). More importantly, Fig. 2(b) reveals the environmental cost associated with pursuing higher SS/SH ratios; the relative CO_2 footprint of the activator increases continuously and in proportion to the rising SS/SH ratio. This is because Na_2SiO_3 is industrially produced by melting silica sand with soda ash at temperatures ranging between 1100 and 1400°C, generating approximately 1.0 to 1.5 kg of CO_2 per kg of silicate produced. A study conducted by (Fořt et al., 2024) demonstrated that, under European production conditions, Na_2SiO_3 is responsible for approximately 57% of the acidification potential and 61% of the associated fossil fuel depletion potential of GPC. This mechanical-environmental trade-off makes activator optimisation both a performance and a sustainability imperative. SS/SH ratios above 2.5 incur disproportionate environmental cost for marginal or negative strength returns.

Solid one-part activator systems, in which pre-dissolved or encapsulated activator is blended with the dry precursor prior to delivery, have attracted significant research interest as a means of simultaneously reducing on-site handling risks, proportional activator dosage, and the CO_2 burden of liquid silicate transport (Qin et al., 2022). Compressive strengths competitive with conventional two-part systems have been reported under ambient curing conditions for FA/GGBFS one-part formulations, though setting time control and activator dissolution uniformity require further development before large-scale structural deployment (Qin et al., 2022; Tahwia et al., 2024).

5. Mix Design Methodologies

No internationally standardised mix design procedure for geopolymer concrete currently exists, and this absence has been repeatedly identified as one of the most significant barriers to widespread structural adoption (Nodehi & Taghvaee, 2022; Tahwia et al., 2024). Table 3 maps the five broad methodological frameworks that appear in the reviewed dataset, ranging from practitioner-familiar target-strength approaches to computationally intensive multi-objective machine learning frameworks. A critical limitation common to the majority of published mix design studies is the use of single-source precursors optimised within a single laboratory, and this practice produces mix proportions that may not transfer reliably to other FA or GGBFS sources with different reactive glass content, particle size distribution, or alkali demand (Khasawneh, 2025; Kolade et al., 2025). Machine learning approaches partially address this limitation by training on multi-source datasets, but the largest published FA/GGBFS databases contain fewer than 1,500 data points, which is insufficient for robust generalisation across the full compositional space of globally available precursors (Golafshani et al., 2024; Kong et al., 2025).

Table 3
Mix design methodologies for binary FA/GGBFS geopolymer concrete

Methodology	Principle	Key Parameters	Strengths / Limitations	Representative Studies
Target-Strength-Based	Analogous to OPC practice; 28-day compressive strength (fc_{28}) is the primary design target	w/b ratio; FA/GGBFS ratio; NaOH molarity; SS/SH ratio	Familiar to practitioners; rapid to implement. Limited optimisation of durability or CO_2 performance	(Hussein & Fawzi, 2021; Samantasinghar & Singh, 2019)
Performance-Based	Targets mechanical, durability, and shrinkage properties simultaneously	fc_{28}; chloride diffusivity; drying shrinkage; w/b ratio	More comprehensive and structurally relevant. Requires a larger experimental programme	(Nodehi & Taghvaee, 2022; Wong, 2022)
Response Surface Methodology (RSM)	Statistical design of experiments (DoE); polynomial response models fitted to measured properties	FA/GGBFS ratio; NaOH molarity; SS/SH ratio; curing temperature	Efficient for 2–4 variables; reduces experimental programme size. Single-objective at a time	(Emarah, 2025; Shahmansouri et al., 2021; Zhao et al., 2024)
Machine Learning / AI	ANN, CNN, gradient boosting trained on multi-source datasets to predict strength and durability	All mix parameters; R^2 > 0.93 achievable for fc	Highest predictive accuracy for multi-variable systems. Requires large datasets (> 1,500 data points) for robust generalisation	(Golafshani et al., 2024; Kong et al., 2025; Wudil et al., 2024)
Multi-Objective Optimisation (CNN-RSM-NSGA-III)	Hybrid ML + RSM + evolutionary optimisation for simultaneous fc, cost, and CO_2 targets	FA/GGBFS ratio; NaOH molarity; SS/SH ratio; LCA boundary	Pareto-front solution; FA/GGBFS ≈ 1:3 identified as balanced design point. Computationally demanding	(Kong et al., 2025; Tushar et al., 2025)

The target-strength-based approach, directly analogous to OPC mix design practice, treats the 28-day compressive strength as the sole design output and adjusts FA/GGBFS ratio, NaOH molarity, SS/SH ratio, and w/b ratio empirically to achieve a specified strength grade (Hussein & Fawzi, 2021). While accessible to practitioners familiar with conventional concrete design, this approach provides no systematic guidance on durability or environmental performance and is inadequate for high-exposure structural applications where chloride diffusivity or acid resistance must also be controlled. The performance-based approach addresses this limitation by simultaneously targeting mechanical properties, durability, and shrinkage. However, it requires a much more extensive experimental program and is best implemented within an RSM or ML framework (Wong, 2022). Response Surface Methodology (RSM) has proven particularly effective in binary FA/GGBFS mixes, enabling the simultaneous and efficient optimization of compressive strength, workability, and drying shrinkage within a limited experimental range through polynomial response models (Emarah, 2025). (Shahmansouri et al., 2021) applied RSM to GGBFS-based GPC incorporating silica fume, demonstrating that the combined effect of GGBFS and NaOH concentration on strength exhibits a highly nonlinear nature.

RSM is most efficient when limited to 2–4 input variables; beyond this, the polynomial approximation breaks down and machine learning models offer superior accuracy.

Machine learning approaches have demonstrated the highest predictive accuracy for GPC compressive strength, as shown in Fig. 3(b). (Kong et al., 2025) developed a CNN-RSM-NSGA-III hybrid framework that achieved R^2 = 0.937 and RMSE = 4.73 MPa for 28-day compressive strength of FA/GGBFS GPC, with SHAP (SHapley Additive exPlanations) analysis identifying FA content as the primary predictor, followed by NaOH concentration and slag content, which is a ranking consistent with the sensitivity analysis in Fig. 3(a). (Golafshani et al., 2024) applied ensemble boosting algorithms to a multi-source geopolymer recycled aggregate concrete dataset, achieving less than 6% mean absolute percentage error.

Regardless of the methodology employed, four parameters consistently emerge as the dominant design variables for ambient-cured FA/GGBFS GPC, as illustrated in Fig. 3(a). The FA/GGBFS mass ratio, which is the single most influential parameter governing both strength and environmental performance; NaOH molarity (8–14 M); SS/SH mass ratio (1.5–2.5); and water-to-binder ratio (0.35–0.45). Together, these four parameters account for more than 85% of the observed variance in compressive strength (Emarah, 2025; Kong et al., 2025); this underscores that any mix design approach failing to systematically vary all four of these parameters may yield results that are ideal at the local level but cannot be generalized or transferred globally.

6. Mechanical Properties

6.1 Compressive Strength

Synthesis of compressive strength dataset demonstrates that binary FA/GGBFS GPC under ambient curing achieves 28-day strengths in the range 45–85 MPa, with system performance strongly dependent on GGBFS content, NaOH molarity, SS/SH ratio, and w/b ratio. Slag-rich systems (≥ 50% GGBFS) consistently exceed 70 MPa, while FA-dominant formulations (≥ 80% FA) without elevated curing typically achieve 45–55 MPa, which is a range broadly meeting the requirements of normal-strength structural concrete per ACI 318 − 19 (ACI Committee 318, 2019). The distribution of compressive strength by system category is summarised in Fig. 4(a). The positive relationship between slag content and compressive strength is one of the most consistently reported findings in the binary FA/GGBFS literature, consistent with the mechanistic understanding that slag addition increases C-A-S-H gel content and drives productive geopolymerization at ambient temperature (Samantasinghar & Singh, 2019; Zhao et al., 2024). (Hardjito et al., 2004) established the foundational baseline for heat-cured Class F FA GPC at 44–67 MPa; subsequent binary FA/GGBFS formulations have consistently extended this range upward through ambient curing by exploiting the reactive calcium contribution of GGBFS (Deb et al., 2014; Lee & Lee, 2013).

The effect of NaOH molarity on compressive strength is non-monotonic, as established in Section 5, namely that increasing from 8 M to 12 M consistently improves strength across the reviewed dataset, but further increase to 14 M reduces strength by 5–15%, attributed to excess Na^+ disrupting gel network formation (Hussein & Fawzi, 2021; Verma & Dev, 2021). (Verma & Dev, 2021) further demonstrated that the combined effect of GGBFS replacement level and curing duration is highly interactive, showing that at 50% GGBFS, extending ambient curing from 28 to 90 days increases strength by 8–12%, while at 80% GGBFS the gain is negligible because C-A-

S-H formation is already substantially complete at 28 days. Table 4 summarizes 28-day compressive strength data for ternary FA/GGBFS geopolymer concrete

Table 4
28-day compressive strength

System	NaOH (M)	SS/SH	w/b	Curing	f_{28} (MPa)	Reference
100% Class F FA	14	2.5	0.45	60°C / 24h	48–64	Hardjito et al. (2004)
80% FA + 20% GGBFS	10	1.5	0.40	Ambient	45–55	Samantasinghar & Singh (2019); Deb et al. (2014)
60% FA + 40% GGBFS	10	2.0	0.40	Ambient	62–70	Kong et al. (2025); Lee & Lee (2013)
55% FA + 45% GGBFS	8	1.5	0.38	Ambient	62–78	Verma & Dev (2021)
50% FA + 50% GGBFS	10	2.0	0.35	Ambient	70–80	Mehta & Siddique (2020); Verma & Dev (2022)
30% FA + 70% GGBFS	10	1.5	0.35	Ambient	70–85	Zhao et al. (2024)
100% GGBFS	10	1.0	0.40	Ambient	60–75	(Taher et al., 2024)
FA/MK/GGBFS (ternary)	12	2.0	0.38	Ambient	63–83	(Amin et al., 2022)
GGBFS + Silica Fume (high-strength)	12	2.0	0.30	Ambient	80–105	Paruthi et al. (2024)
Compiled range (ambient binary)	**8–14**	**1.5–2.5**	**0.33–0.45**	**20–25°C**	**45–85 MPa (≥ 50% GGBFS: 70–85 MPa)**	--

6.2 Flexural Ductility and Fibre Reinforcement

The flexural and splitting tensile strengths FA/GGBFS GPC generally mirror its compressive strength. However, the tensile/compressive strength ratios differ from those prescribed in design codes for OPC and should not be directly applied to the structural elements of GPC. The flexural/compressive strength ratio of GPC typically ranges between 0.10 and 0.14; while these values are consistent with those of OPC, they exhibit greater variability due to their sensitivity to the chemical activator composition of the gel network and the reactivity of the raw materials (Amin et al., 2022; Taher et al., 2024). (Castel & Foster, 2015) showed this through bond strength measurements, reporting that the bond strength between deformed reinforcing steel and blended slag/Class F FA GPC is equal to or higher than the corresponding values for equivalent OPC.

Fiber reinforcement in GPC significantly transforms the post-crack response from brittle to ductile, thereby enabling its classification as high-performance fiber-reinforced concrete (HPFRCC) when appropriate fiber ratios are used (Naaman & Reinhardt, 2007). Steel fiber volumes of 1–2% by volume lead to increase in fracture energy,

as well as significant improvements in energy absorption and seismic toughness, in column-beam joint applications (Qin et al., 2022).

Hybrid fiber systems (combine macro steel fibers to bridge cracks with micro polypropylene fibers to control early-stage shrinkage cracks) offer combined benefits that neither fiber type can provide on its own. Basalt fibers offer as a corrosion-resistant alternative to steel fibers; at a volume fraction of 1–2%, they increase flexural strength by 20–40% while retaining their inherent alkali resistance, an advantage not found in E-glass fibers within a high-pH GPC environment (Qin et al., 2022).

6.3 Elastic Modulus, Shrinkage, and Deformation

As shown in Fig. 4(b), it was observed that the modulus of elasticity of FA/GGBFS GPC is consistently lower than that of OPC at equivalent compressive strength. Nath and Sarker (2014) determined that this difference amounted to 25–30% lower than OPC of the same strength across various binary blend mixtures cured at room temperature, and attributed this to the gel microstructure and aggregate-binder interaction characteristics, which differ significantly from the C-S-H matrix of OPC paste.

They further proposed a GPC-specific expression (Eq. 2), which provides substantially better agreement with experimental data than the ACI 318 − 19 expression. (Mehta et al., 2020) confirmed a similar shortfall of 15–25% in FA/GGBFS alkali-activated concrete. As illustrated in Fig. 4(b), the ACI 318 − 19 expression (Eq. 1) systematically overestimates measured GPC modulus values by 15–25% across the reviewed strength range of 45–85 MPa (ACI Committee 318, 2019). This discrepancy has direct structural design implications as serviceability limit-state deflection calculations using the ACI 318 − 19 modulus expression calibrated to OPC concrete may underestimate deflections in GPC beams by 15–25%, a concern particularly relevant to lightly reinforced slabs and long-span floor systems where serviceability governs design.

$$\mathrm{Ec} \;=\; 4{,}730\sqrt{\mathrm{fc}},\ \mathrm{MPa} \qquad (1)$$

$$\mathrm{Ec} \;=\; 3{,}320\sqrt{\mathrm{f_c}} \;+\; 6{,}900\,\mathrm{MPa}$$

2

Drying shrinkage is a recognised concern in FA-rich binary systems. The shrinkage mechanism in GPC differs fundamentally from that in OPC concrete, as GPC shrinkage is dominated by gel syneresis, which is the internal expulsion of water from the gel network during polycondensation, rather than by capillary tension in drying pores. (Samantasinghar & Singh, 2019). This mechanistic difference has a critical practical implication, namely that shrinkage reducing admixtures (SRA) calibrated for OPC concrete through capillary tension reduction cannot be assumed effective in GPC without independent verification, as demonstrated by (Rashad, 2014). The addition of slag constitutes a more reliable and effective strategy for reducing shrinkage in binary systems, as strongly supported by the examined experimental data. Nevertheless, long-term creep behavior remains poorly characterized beyond two-year measurement horizons; this represents a critical gap for prestress (Nodehi & Taghvaee, 2022; Wasim et al., 2021).

7. Durability Performance

7.1 Acid and Sulphate Resistance

The resistance of GPC incorporating Class F fly ash to sulfuric acid and sulfate attack is the most prominent feature in terms of durability, providing the strongest mechanical distinction from OPC.

In OPC concrete, acid attack occurs through the dissolution of portlandite $Ca(OH)_2$ and C-S-H, the two calcium-bearing compounds responsible for the alkalinity of the paste. This process yields soluble calcium salts, and in sulfate, results in the formation of expansive ettringite (Bakharev, 2005; Mehta & Siddique, 2017). In low-calcium FA GPC, the portlandite is entirely absent, and the content of the C-A-S-H phase is low; furthermore, the charge of its N-A-S-H network is electrically balanced by sodium rather than calcium, rendering it significantly less susceptible to proton exchange processes and ion leaching (Mehta & Siddique, 2017). Samples immersed in 5% H2SO4 for twelve months exhibited a strength loss of less than 5%, whereas equivalent OPC samples lost 40–70% (Boutkhil et al., 2024). This acid resistance makes the Class F FA GPC particularly suitable for wastewater treatment infrastructure, marine foundations, and industrial flooring exposed to acidic process byproducts.

The sulphate resistance of FA/GGBFS GPC depends critically on the type of sulphate salt and the composition of the raw material; these dependencies must not be conflated in general descriptions of GPC durability. A study by (Bakharev, 2005) demonstrated that Class F FA GPC activated with NaOH exhibited a 4% increase in strength after 5 months in a 5% Na_2SO_4 solution. This effect is attributed to the continuation of the geopolimerization process, which is enhanced by the high-pH environmen. In contrast, samples prepared using a mixed activator of NaOH/KOH showed a 65% decrease in strength, indicating that the chemical composition of the activator is as critical as precursor type in governing sulphate response.

(Ismail et al., 2013) highlighted a significant difference in microstructure. Geopolymers synthesized from FA/slag exhibit substantial degradation in $MgSO_4$ solution, specifically through the formation of gypsum and associated expansion effects. This disparity is attributed to the fact thatMg^{2+} exchange with Na^+ within the gel structure, thereby destabilizing the matrix. Slag-rich GPC (> 60% GGBFS) can generate limited amounts of ettringite under aggressive exposure to Na_2SO_4 and NaCl at elevated temperatures due to its C-A-S-H content. This confirms that sulphate resistance is more pronounced in FA-dominated formulations and must be evaluated with reference to both the precursor composition and the specific aggressive ion (Ismail et al., 2013; Yazıcı & Karagöl, 2024). (Singh & Rajhans, 2025) reported a residual compressive strength of 86.4% after 6 months in a medium containing 3% HCl, with surface morphology stability confirmed by SEM. This further demonstrates the durability of the geopolymer network across multiple aggressive acidic environments.

7.2 Chloride Penetration and Corrosion Resistance

Compared to OPC paste at an equivalent w/b ratio, the dense geopolymer gel matrix significantly reduces the effective chloride diffusion coefficient through two simultaneous mechanisms: reduced physical permeability via a more tortuous pore network, and chemical chloride binding within the N-A-S-H gel through interactions with aluminate species (Wong, 2022; Wasim et al., 2021). Through accelerated chloride migration tests, Mehta and Siddiq (2020) confirmed that the combined effects of gel densification resulting FA/GGBFS GPC with 40–50% GGBFS derived C-A-S-H and the binding capacity of the aluminosilicate geopolymer network.

RCPT values below 2,000 coulombs (low penetrability class per ASTM C1202) are consistently reported for well-proportioned binary FA/GGBFS systems (Hamsashree et al., 2024). Paruthi et al. (2024) reported RCPT values below 200 coulombs for GGBS + SF GPC, which falls into the very low penetrability category, confirming that silica fume additions further densify the pore structure. (Lokesha et al., 2025) demonstrated low chloride

diffusivity in FA/GGBFS GPC with recycled aggregates, confirming that the geopolymer chloride resistance advantage is maintained even with secondary aggregate sources.

A notable contradiction in the literature concerns the relationship between NaOH molarity and chloride resistance. Wong (2022) reported the opposite trend for different precursor combinations. This contradiction is mechanistically explicable: high-calcium FA (Class C) produces more C-A-S-H at higher activator concentration, densifying the matrix, while low-calcium FA (Class F) generates predominantly N-A-S-H whose pore connectivity increases at excess alkali concentration. Precursor-specific testing is therefore essential before specifying chloride resistance targets for a given FA/GGBFS combination, and generic RCPT targets from one precursor source should not be applied to another without independent verification (Wasim et al., 2021).

7.3 Thermal and Fire Resistance

The thermal and fire resistance of GPC is, alongside its acid resistance, the property most clearly differentiating it from OPC concrete under extreme structural loading conditions, as illustrated in Fig. 5(a). The N-A-S-H network does not undergo the endothermic dehydration and $CaCO_3$ decomposition reactions that weaken OPC paste above 300°C, and does not generate free calcium oxide that hydrates expansively and causes spalling upon re-wetting after fire exposure (Alahmari et al., 2023; Taher et al., 2024). FA-dominant GPC retains over 90% of its initial strength at 800°C and maintains structural coherence approaching 1,000°C, as confirmed by (Khasawneh, 2025) and Alahmari et al. (2023) across multiple independent experimental programmes. GGBFS-rich systems show somewhat lower thermal retention, as the C-A-S-H component is less thermally stable than N-A-S-H above 400°C, but binary FA/GGBFS systems with 30–50% slag still substantially outperform OPC concrete above 300°C (Taher et al., 2024; Alahmari et al., 2023). Polypropylene fibre additions at 0.1–0.3 vol% are effective in mitigating explosive spalling in GPC under rapid heating rates: the fibres melt at approximately 165°C, creating interconnected pressure relief channels that allow pore steam pressure to dissipate before reaching critical levels (Qin et al., 2023). This spalling mitigation strategy is directly transferable from OPC concrete practice and does not require modification of GPC mix design beyond fibre dosage optimisation. GPC members in equivalent fire rating categories may require significantly less passive fire protection than OPC concrete equivalents, with weight and cost savings particularly relevant in high-rise and tunnel applications; however, formal structural fire engineering assessment per EN 1992-1-2 remains required for project-specific implementation (Tahwia et al., 2024).

7.4 Freeze–Thaw, Carbonation, and Water Absorption

The freeze-thaw resistance of FA/GGBFS GPC is generally positive, but it is more variable than its resistance to acids and fire. many studies confirm minimal strength loss after 300 freeze-thaw cycles in well-cured binary FA/GGBFS mixes; this is attributed to reduced capillary porosity and gel pore network, which decrease the volume of freezable water. (Wong, 2022; (Hamsashree et al., 2024). Nevertheless, GPC mix designs, particularly those with high w/b ratios or incomplete activation, suffer greater freeze–thaw damage than OPC controls under severe cycling (> 200 cycles). This highlight a mix-design sensitivity that makes site testing preferable to generic durability assumptions (Cong et al., 2024; Hamsashree et al., 2024).

In GPC enriched with FA carbonation occurs at higher rates compared to OPC. This is because the N-A-S-H pore solution carries lower alkaline buffering capacity, typically pH 10–11, compared to the $Ca(OH)_2$ saturated pore solution of OPC paste (pH 12.5–13.5), which provides a large pH reserve against CO_2 ingress (Bernal et al.,

2013). As illustrated in Fig. 5(b), the carbonation depth follows square root of time kinetics (Eq. 3), and is primarily governed by the activator modulus, slag replacement ratio, and curing conditions.

$$d = k\sqrt{t} \qquad (3)$$

Zhao et al. (2024) derived carbonation coefficients k of approximately 4.2 mm/√year for FA-dominant GPC and approximately 1.9 mm/√year for 70% GGBFS binary GPC under accelerated testing, demonstrating that slag addition substantially improves carbonation resistance by increasing pore solution alkalinity through C-A-S-H formation. The RILEM TC 247-DTA accelerated carbonation protocol (1% CO_2, 65% RH) has been validated for FA/GGBFS GPC through a multi-laboratory round robin exercise (Gluth et al., 2020), providing a credible standardised test method for carbonation assessment. For reinforced GPC elements in outdoor environments, carbonation data from Fig. 5(b) confirm that FA-dominant formulations require increased concrete cover (5–10 mm above OPC code minimums) to maintain equivalent rebar corrosion protection, while 70% GGBFS systems achieve carbonation depths comparable to OPC concrete at standard design cover depths of 30–50 mm (Zhao et al., 2024). Table 5 summarized the comparative durability performance of binary FA/GGBFS geopolymer concrete versus OPC concrete across principal degradation mechanisms, compiled from high- and medium-confidence studies in the reviewed dataset, and the comprehensive comparative durability picture is shown in Fig. 6.

Table 5
Comparative durability performance of binary FA/GGBFS geopolymer concrete versus OPC concrete.

Durability Aspect	GPC Performance	OPC Performance	References
H_2SO_4 (5%, 12 months)	< 5% strength loss; dense N-A-S-H matrix intact	40–70% strength loss; matrix disintegrates	Mehta & Siddique (2017); Bakharev (2005); Boutkhil et al. (2024)
Na_2SO_4 (FA-dominant)	No ettringite; negligible expansion; strength stable or slight gain	> 10% mass gain; expansive cracking	Bakharev (2005); Ismail et al. (2013); Yazici et al. (2024)
$MgSO_4$ (FA/GGBFS)	Limited gypsum formation in slag-rich systems; Na_2SO_4 exposure more benign	Significant expansion, cracking; ettringite and gypsum	Ismail et al. (2013); Yazici et al. (2024)
HCl (3%, 6 months)	Residual strength 86.4%; stable surface	Severe erosion and spallation	Singh & Rajhans (2025); Wong (2022)
Chloride (RCPT, ASTM C1202)	Low–Medium (< 2,000 C); low diffusivity; FA/GGBFS 30–50% optimal	Moderate–High (2,000–4,000 C)	(Hamsashree et al., 2024) Mehta & Siddique (2020)
High Temperature (800°C)	≥ 90% strength retained; N-A-S-H stable; C-A-S-H partially degrades	30–50% retained; C-S-H decomposes above 300°C	(Khasawneh, 2025) Alahmari et al. (2023); Taher et al. (2024)
Freeze–Thaw (300 cycles)	Variable; minimal in well-cured binary systems; mix-design sensitive	Significant mass loss and cracking in non-air-entrained concrete	(Hamsashree et al., 2024)Cong et al. (2024); Wong (2022)
Carbonation	Higher rate in FA-dominant systems ($k \approx 4.2$ mm/√year); improved with GGBFS addition	Lower rate due to $Ca(OH)_2$ buffering ($k \approx 1.5$ mm/√year)	Zhao et al. (2024); Bernal et al. (2013)
Water Absorption	Generally, < 5% by mass in well-cured systems	5–12% for normal-strength OPC concrete	Alahmari et al. (2023); Samantasinghar & Singh (2019)
Drying Shrinkage	Higher in FA-rich systems; gel syneresis mechanism; reduced with slag addition	Lower for normal-strength OPC; capillary tension mechanism	Samantasinghar & Singh (2019)
Abrasion Resistance	Superior, hard, dense gel matrix	Moderate	Wong (2022); Qin et al. (2023)

8. Sustainability and Economics

8.1 Life-Cycle CO_2 Emissions

Table 6 summarized the CO_2 emission data from peer-reviewed LCA studies, all adopting a cradle-to-gate system boundary aligned with EN 15804 and ISO 14040/44, with the functional unit defined as one cubic metre of concrete at a specified 28-day compressive strength. The studies are illustrated in Fig. 7. Differences in geographic allocation, electricity grid carbon intensity, transport distances, and activator-to-precursor ratios

contribute to the reported variability of 35–65% CO_2 reduction across the dataset (Tushar et al., 2025; Cong et al., 2024).

The sensitivity of the CO_2 reduction to activator chemistry is the most important finding across the LCA dataset. Shi et al. (2021) demonstrated through multivariate impact correlation analysis that the activator solution to FA ratio contributes up to 87% of GPC carbon emissions, confirming activator reduction as the single most effective lever for maximising CO_2 savings. The contrast between the low activator FA GPC scenario (148 kg CO_2/m³, 63% reduction) and the high-activator scenario (260 kg CO_2/m³, 35% reduction) in (Shi et al., 2021) illustrates that the choice of activator dosage alone can determine whether GPC achieves a transformative or modest environmental improvement over OPC concrete.

Table 6
CO_2 emissions for FA/GGBFS-based geopolymer concrete systems versus OPC concrete

GPC System / Study	GPC CO_2 (kg/m³)	OPC CO_2 (kg/m³)	Reduction (%)	Reference
FA/GGBFS GPC (SimaPro 9.4, Monte Carlo)	228	397	43%	Tushar et al. (2025)
Fly Ash GPC (high activator ratio)	260	397	35%	Shi et al. (2021)
Fly Ash GPC (low activator ratio)	148	397	63%	Shi et al. (2021)
FA-SF geopolymer (service-life LCA)	~ 200	~ 400	~ 50%	Cong et al. (2024)
Zeolite + blast furnace slag GPC	205–240	354	32–40%	Amari et al. (2024)
Mine tailings GPC (Norway)	116–142	~ 410	57–65%	(Brekke & O'Born, 2025)
FA/GGBFS GPC (SimaPro, ReCiPe H)	~ 215	~ 390	~ 45%	(Polusani et al., 2025)
CDW fully recycled concrete geopolymer	165	380	~ 57%	(Rahimpour & Esmaeili, 2025)
GGBFS-based GPC (meta-analysis)	~ 180	~ 390	~ 54%	(Martínez & Miller, 2025; Shehata et al., 2022)
MK-based GPC	High GWP	~ 400	20–45%	(Turner & Collins, 2013)

Beyond global warming potential, multi-criterion LCA consistently reveals that Na_2SiO_3 production dominates GPC acidification potential (~ 57%) and fossil resource depletion (~ 61%) due to the energy-intensive Solvay process used to manufacture soda ash, a key raw material in silicate production (Fort et al., 2024). Fort et al. (2024) further demonstrated that GPC's ozone depletion potential can be up to twelve times higher than OPC concrete, attributable to carbon tetrachloride emissions from the chlor-alkali process used in industrial NaOH manufacturing. These findings confirm that single-indicator GWP comparisons are insufficient for a complete environmental assessment of GPC, and that multi-criterion LCA frameworks covering acidification, eutrophication, fossil depletion, and ozone depletion alongside GWP must become standard practice for GPC environmental benchmarking (Meshram & Kumar, 2022; Wudil et al., 2024). Replacing chemically manufactured

Na_2SiO_3 with waste-derived activators, such as rice husk ash silica, glass cullet alkali, or calcined waste paper sludge, is the highest-priority environmental intervention for reducing GPC's non-GWP impact categories (Passuello et al., 2017; Qin et al., 2022).

8.2 Circular Economy and Economic Performance

GPC is a circular economy material at multiple simultaneous scales. It transforms post industrial waste streams (FA and GGBFS) into structural products, eliminates the landfill burden and leachate risk associated with current FA and GGBFS disposal, displaces the most carbon-intensive binder in construction, and has demonstrated capacity to immobilise toxic heavy metals, including arsenic, lead, chromium, and barium within the geopolymer gel matrix, converting contaminated mining tailings into inert, structurally useful construction materials (Brekke & O'Born, 2025; Lokesha et al., 2025; Shehata et al., 2022). LCA studies have confirmed material reuse fractions approaching 70% in optimised FA/GGBFS GPC formulations, figures consistent with EU Circular Economy Action Plan targets and directly supporting the Sustainable Development Goals SDG 12 (Responsible Consumption) and SDG 13 (Climate Action) ((Shehata et al., 2022); (Khasawneh, 2025)). Roychand et al. (2023) further demonstrated that CO_2 mineralisation during GPC production, through the reaction of atmospheric or industrial CO_2 with the alkaline activator solution, offers an additional carbon sequestration pathway not available in OPC concrete systems.

Turner and Collins (2013) established the fundamental quantitative framework for comparing the carbon footprints of GPC and OPC; this framework was subsequently refined through Monte Carlo uncertainty analysis (Tushar et al., 2025) and expanded by Amari et al. (2024). Amari et al. (2024) demonstrated that under North African production conditions a zeolite-blast furnace slag geopolymer exhibits a 32–40% reduction in CO_2 emissions compared to OPC.

A comprehensive meta-analysis conducted by (Martínez & Miller, 2025), which examined 38 published life cycle assessment studies, confirmed a central estimate of approximately 54% CO_2 emission reduction when GGBFS-based GPC is utilized. It was noted that the results varied between 20% and over 80%, depending on system boundary assumptions, geographical context, and activator dosage. The anticipated decline in coal-fired energy generation in Europe creates a structural vulnerability in the supply of FA, necessitating the proactive development of alternative raw materials. Calcined clays are particularly promising due to their global geological abundance, while CDW glass, agricultural silica residues, and geologically diverse volcanic materials represent additional pathways (Qin et al., 2022); (Islam et al., 2025).

In terms of material costs, market prices for improved GPC are approximately 20–40% higher than those for equivalent OPC in most markets; the primary reason for this is that chemical activators account for 40–60% of the total material cost of improved GPC in standard formulations (Martínez & Miller, 2025). Nevertheless, for infrastructure exposed to acids and harmful chemicals, the life-cycle cost advantage of improved GPC is significant, as reduced maintenance, extended service life, and the elimination of protective coating systems generate a positive net present value at realistic discount rates (Khasawneh, 2025); (Shehata et al., 2022); Cong et al., 2024). Mishram and Kumar (2022) demonstrated that, within a manufacturing context in India, even at current material prices, GPC achieves life-cycle cost parity with OPC when waste disposal credits for FA and GGBFS are incorporated into a full-cost accounting analysis; this finding is significant in terms of circular economy incentive structures.

9. GPC Performance Classification Matrix

One of the key contributions of this review is the proposed GPC Classification Matrix (Table 7), which provides a five-tiered systematic framework linking raw material chemistry, dominant gel type, mechanical performance, durability class, curing requirements, and recommended structural applications. This matrix addresses the critical and widely observed lack of a systematic specification framework for geopolymer concrete, a deficiency identified in the peer-reviewed scientific literature as one of the major barriers to the widespread adoption of this concrete in structural applications (Nodehi & Taghvaee, 2022; Rossi et al., 2023). In the recent comprehensive assessment of standardization pathways for alkali-activated materials, Rossi et al. (2023) identified the absence of a performance-based classification as the most significant conceptual gap hindering the development of geopolymer concrete specifications accessible to engineers. The matrix proposed herein directly addresses this need.

The five levels (GPC-I to GPC-V) are defined based on the ratio of FA/GGBFS ratio; they are further distinguished by the dominant gel type produced, the 28-day compressive strength range, the durability class (DC-1 to DC-5, in accordance with the exposure condition classification principles of EN 206), the minimum curing requirements necessary to ensure reliable strength, and, finally, the recommended structural applications. The DC classification adopted herein is consistent with the exposure condition severity classes of EN 206:2021 and with the performance-based testing recommendations for durability assessment published by RILEM Technical Committee TC 247-DTA (Provis & Van Deventer, 2014).

Table 7
Proposed GPC Performance Classification Matrix.

Tier	FA/GGBFS Ratio	Dominant Gel Type	f_{28} Range (MPa)	Durability Class	Curing Required	Recommended Application	Data Sources (verified)
GPC-I	80:20 to 70:30	N-A-S-H dominant	38–55	DC-1 (mild)	60°C/24h or >7d ambient	Non-structural; paving; road base	Hardjito et al. (2004); (Samantasinghar & Singh, 2019)
GPC-II	70:30 to 60:40	N-A-S-H / C-A-S-H hybrid (FA-rich)	50–68	DC-2 (moderate)	Ambient (14–28d) or 40°C/24h	Light structural; slabs; pavements	Lee & Lee (2013); Deb et al. (2014)
GPC-III	60:40 to 50:50	Balanced N-A-S-H / C-A-S-H	62–78	DC-3 (severe)	Ambient (28d)	Standard structural; columns; beams	(Hussein & Fawzi, 2021)Mehta & Siddique (2020); Verma & Dev (2021)
GPC-IV	50:50 to 30:70	C-A-S-H dominant	72–85	DC-4 (very severe)	Ambient (28d)	High-strength structural; marine; wastewater	Zhao et al. (2024); Mehta & Siddique (2020); Verma & Dev (2022)
GPC-V	With SF + steel fibres (GGBFS-rich)	Dense C-A-S-H / N-A-S-H hybrid	> 80	DC-5 (extreme)	Ambient or 60°C/24h (steam opt.)	High-strength structural; blast; seismic	Paruthi et al. (2024); (Amin et al., 2022); Nath & Sarker (2014)

The transition from GPC-I to GPC-IV, reflecting an increase in GGBFS content, shifts the dominant gel type from N-A-S-H to C-A-S-H. This gradually enhances the strength achieved under ambient curing conditions, reduces dependence on thermal treatment, and improves chloride resistance and carbonation performance. GPC-I (with FA/GGBFS ratios ranging from 80:20 to 70:30) represents the minimum practical binary blend suitable for ambient curing. GPC-II (70:30 to 60:40) attains a strength of 50–68 MPa under ambient or moderate thermal treatment conditions and, consistent with data from Lee & Lee (2013) and Deb et al. (2014), is suitable for light structural elements such as slabs and pavements.

The GPC-III classification (60:40 and 50:50) represents the balanced design range. With a balanced gel matrix composed of N-A-S-H and C-A-S-H, this classification achieves a compressive strength of 62–78 MPa under ambient curing conditions, while simultaneously providing controllable compressive strength, durability, and setting time. This level corresponds directly to the design point where the ratio of FA/GGBFS is close to 1:1, making it suitable for standard structural applications (e.g., columns, bridges, and foundations). This classification is based on experimental data provided by Mehta and Siddique (2020) and Verma and Dev (2021). The GPC-IV classification (50:50 and 30:70) is characterized by high slag content and C-A-S-H dominance. Attaining a strength of 72–85 MPa under ambient conditions, this product becomes suitable for high-strength construction, marine, and wastewater treatment applications where both high strength and resistance to chlorides and acids are required (Zhao et al., 2024; Verma & Dev, 2022). The advantage of chloride resistance is

maximized at this level as verified by transport property tests conducted by Mehta & Siddique (2020), the combination of high C-A-S-H content and a dense gel microstructure.

The GPC-V incorporates silica and steel fibers into a matrix rich in GGBFS, targeting a compressive strength exceeding 80 MPa and a DC-5 durability level for extreme exposure classes, including blasts, earthquakes, and combined chemical attacks. Paruthi et al. (2024) confirmed a range of 80–105 MPa for the GGBS + SF ambient cured GPC; meanwhile, (Amin et al., 2022) reported a range of 63–83 MPa for ternary FA/MK/GGBFS systems.

The proposed classification does not constitute a design standard and must be validated against a wider, geographically diverse experimental dataset before adoption in practice. In particular, the durability class assignments (particularly DC-3 through DC-5) require validation through standardised long-term exposure testing per RILEM TC 247-DTA protocols across the full range of precursor sources before formal specification. The matrix is presented as a conceptual tool intended to stimulate structured discussion within RILEM TC 283-CAM, ACI Committee 232, and ISO TC71 working groups currently developing performance-based design guidance for alkali-activated and geopolymer concrete (Rossi et al., 2023; Provis & van Deventer, 2014;). Performance-based standards, which specify required f_c, durability class, and service-life thresholds rather than binder chemistry prescriptions, are the correct regulatory pathway for enabling GPC in structural practice without imposing OPC-derived compositional constraints (Wasim et al., 2021).

10. Engineering Application and Design Guidance

The translation of GPC research findings into practical structural design requires explicit guidance on the application of existing codes to geopolymer systems. Table 8 maps current GPC performance data from the reviewed dataset against the requirements of ACI 318 − 19 (ACI Committee 318, 2019), EN 1992-1-1 (Eurocode 2), and identifies the adjustments necessary for each parameter. Three primary challenges are identified.

First, the elastic modulus. The ACI 318 − 19 expression (Eq. 1) and the Eurocode 2 expression (Eq. 3) are both calibrated to OPC concrete and systematically overestimate the elastic modulus of FA/GGBFS GPC by 15–25% across the strength range of 45–85 MPa. The GPC expression (Eq. 2), experimentally derived by Nath & Sarker (2014) for binary FA/GGBFS GPC ambient-cured, demonstrates a significantly better fit with the experimental dataset examined herein. Consequently, it is recommended for use in place of the ACI 318 − 19 expression for serviceability calculations involving structural GPC elements.

$$\mathrm{Ec} \;=\; 22(\mathrm{fc}/10)^{0.3}\ \mathrm{GPa} \qquad (3)$$

Secondly, concrete cover for carbonation. GPC containing a high volume of FA (≥ 80%) exhibits a higher carbonation coefficient (k) compared to ordinary OPC concrete under equivalent exposure conditions (Zhao et al., 2024). Consequently, the cover depth for XC3/XC4 carbonation exposure classes must be increased by 5–10 mm relative to the minimum specified for OPC concrete, based on project-specific accelerated carbonation tests conducted in accordance with the RILEM TC 247-DTA protocol. Binary FA/GGBFS (≥ 50%) achieve carbonation rates comparable to those of OPC and, therefore, do not require additional cover.

Thirdly, concrete cover for chloride. Binary FA/GGBFS GPC with 30–50% GGBFS exhibits lower chloride permeability compared to OPC with an equivalent w/b ratio. This indicates a potential for a reduction in cover depth within the XS1–XS3 chloride exposure categories. However, before any reduction from the minimum cover

depth required by the code can be established, this reduction must be verified through an RCPT (ASTM C1202) or an accelerated chloride migration test specific to the raw material mix and production source. Generic RCPT values cannot be transferred from one source to another without independent verification.

Table 8
Comparison of GPC-specific design parameters against current ACI 318 – 19 and Eurocode 2 provisions

Design Parameter	ACI 318 – 19 / Eurocode 2 (OPC)	GPC-Specific Value	Proposed Adjustment
Elastic Modulus expression	Eq. (3) and Eq. (4)	Eq. (1)	Use GPC-specific expression (Nath & Sarker, 2017); ACI 318 – 19 overestimates GPC modulus by 15–25%.
Tension-to-compression ratio	f□/f□ = 0.10–0.12 (typical OPC)	f□/f□ = 0.10–0.14 (reviewed literature)	Use GPC-specific relationships; do not apply OPC code expressions without independent verification for the specific FA/GGBFS source
Concrete cover (XC3/XC4 carbonation exposure)	35–45 mm (depends on exposure class)	Increase 5–10 mm for FA-dominant GPC (≥ 80% FA) relative to OPC minimum	Specify cover using site-specific carbonation coefficient k from RILEM TC 247-DTA test; FA-dominant GPC: k ≈ 4.2 mm/√year
Concrete cover (XS1–XS3 chloride exposure)	40–55 mm (depends on exposure class)	Binary FA/GGBFS (30–50% GGBFS) achieves lower diffusivity; potential for reduced cover vs OPC minimum	Verify with RCPT (ASTM C1202) or accelerated chloride migration test before any reduction below code minimum; source-specific testing required
Drying shrinkage limit	EN 1992: 0.03–0.05% (typical OPC)	0.04–0.08% reported for FA-rich GPC; reduced to 0.03–0.05% with ≥ 50% GGBFS	Design using experimentally measured strain from project-specific precursor; standard OPC shrinkage models (CEB-FIP, ACI 209) not directly applicable to GPC
Fire rating (passive fire protection)	Defined by cover depth and member width per EN 1992-1-2	GPC fire performance consistently superior; ≥90% strength retention at 800°C in FA-dominant systems (Khasawneh, 2025)	GPC's superior fire performance may allow reduction of passive fire protection; requires project-specific structural fire engineering per EN 1992-1-2; no GPC-specific fire design standard currently exists

Based on the synthesised dataset, the following preliminary design guidelines are proposed for FA/GGBFS GPC structural applications, pending the development of a dedicated national or international design standard. For normal-strength structural applications (f_c = 25–50 MPa), a FA/GGBFS ratio of 60:40 to 50:50, NaOH molarity of 10–12 M, SS/SH of 1.5–2.0, and w/b of 0.38–0.42 produces reliably ambient-cured concrete meeting most national standard strength class requirements (Kolade et al., 2025; Wong, 2022). For high-strength applications (f_c = 50–80 MPa), increasing GGBFS content to 60–70% and reducing w/b to 0.33–0.38 is the primary lever, with NaOH at 12 M providing the most consistent results across the reviewed literature (Kolade et al., 2025). For durability-critical applications in aggressive chemical environments, FA-dominant formulations (FA ≥ 60%) should be specified to maximise acid and sulphate resistance, while binary 50:50 to 30:70 FA/GGBFS formulations are preferred for chloride and carbonation resistance (Mehta & Siddique, 2017; Zhao et al., 2024). Cover depths for

XC3/XC4 carbonation exposure should be increased by 5–10 mm relative to the OPC minimum for FA dominant GPC systems.

11. Barriers to Adoption

The regulatory barrier is the most consequential single obstacle to mainstream GPC structural adoption. EN 1992, ACI 318, and AS 3600 are written for OPC concrete and specify minimum cement content, maximum w/c ratio, and supplementary cementitious material limits that are conceptually inapplicable to OPC-free binder systems (Nodehi & Taghvaee, 2022). RILEM TC 247-DTA has produced validated accelerated carbonation and chloride testing recommendations for alkali-activated concretes, and Rossi et al. (2023) have comprehensively mapped the pathway from existing standards to structural application. However, no widely adopted national structural design standard for GPC currently exists in Europe, North America, or Asia. Performance-based standards, specifying required f_c, durability class, and service-life thresholds rather than binder chemistry prescriptions, represent the correct and achievable regulatory pathway (Provis & van Deventer, 2014; Davidovits, 2008).

Table 9 summarizes the principal barriers to mainstream structural adoption of FA/GGBFS geopolymer concrete, including root causes and evidence-based mitigation strategies. The precursor variability barrier is equally significant and structurally interconnected with the standards gap, as without standardised reactivity characterisation methods, even a well-written performance-based GPC design standard cannot be implemented reliably. FA from different coal plants can have meaningfully different reactive glass contents (40–70 vol%) and particle size distributions, a variation that cannot be resolved by single-source laboratory optimization ((Kolade et al., 2025); Emarah, 2025). Machine learning-based adaptive mix design, compensating for precursor variability in real time using real-time X-ray fluorescence (XRF) characterisation of incoming batches, represents the most near-term deployable solution for this problem (Kong et al., 2025; Golafshani et al., 2024).

Table 9
Principal barriers to mainstream structural adoption of FA/GGBFS geopolymer concrete

Barrier	Root Cause	Proposed Mitigation	References
Heat-curing dependency (FA-rich systems)	Low CaO in Class F FA slows polycondensation kinetics at ambient temperature	High-slag binary blends (40–60% GGBFS); solid one-part activators; nano-silica seeding	Nath & Sarker (2014); (Kolade et al., 2025)(Qin et al., 2022)
Absent harmonised design standards	OPC-centric codes (EN 1992, ACI 318, AS 3600) specify cement content and w/c limits inapplicable to OPC-free systems	Performance-based standards specifying f, durability class, service life; RILEM TC 247-DTA; ISO TC71; ACI Committee 232	Nodehi & Taghvaee (2022); Rossi et al. (2023);
Activator environmental burden	Na_2SiO_3 produced at 1,100–1,400°C; dominates GPC acidification and fossil depletion	Waste glass silica activators; dry one-part systems; Na_2CO_3 alternative activators	Fort et al. (2024); Passuello et al. (2017); (Qin et al., 2022)
Raw material variability	Source-to-source differences in FA/GGBFS reactive glass content and particle size distribution	Real-time XRF characterisation of incoming batches; ML-adaptive mix design; standardised reactivity testing	Emarah (2025); (Kolade et al., 2025)Kong et al. (2025)
High drying shrinkage (FA-rich systems)	Gel syneresis mechanism; SRA admixtures calibrated for OPC not directly transferable	Slag substitution reduces shrinkage 20–40%; PP fibre additions for crack control	Rashad (2014)
Limited long-term field data (> 25 year)	Relatively recent commercial deployment	International NDT-based monitoring programmes	Wasim et al. (2021); (Nodehi & Taghvaee, 2022)
OHS: high-molarity NaOH on-site	Corrosive activators required during mixing; handling risk for site workers	Encapsulated or pre-dissolved reagent delivery; one-part GPC systems	(Qin et al., 2022) Islam et al., 2025)
Declining coal FA supply (EU 2030)	EU/UK coal phase-out projected by 2030; strategic FA supply vulnerability	Calcined clay; CDW glass; rice husk ash; mine tailings as alternative precursors	(Qin et al., 2022) Islam et al., 2025); (Brekke & O'Born, 2025)

12. Limitations and Future Research

This review has several limitations that must be acknowledged explicitly. The systematic search was restricted to Scopus and Web of Science (Core Collection); studies indexed only in other databases may have been missed, potentially underrepresenting GPC research from Asia, the region with the highest FA and GGBFS production volumes and the most active GPC construction programmes. The compressive strength ranges compiled in Table 4 are drawn from published papers rather than a pooled raw dataset; reporting inconsistencies between studies, particularly regarding specimen geometry (cube vs cylinder), curing duration, and testing protocol, introduce measurement uncertainty that cannot be fully quantified without raw data access. No meta-regression was performed to account for confounding between design variables, meaning the reported univariate trends may partially reflect correlated co-variates (e.g., higher GGBFS content studies also tend to use higher NaOH molarities). All LCA studies reviewed adopted a cradle to gate system boundary, preventing full lifecycle comparison with OPC concrete including use-phase durability benefits. The proposed GPC Performance

Classification Matrix (Table 7) is empirically derived from the reviewed dataset and has not been independently validated against long-term field performance data.

Thus, six research priorities are identified, ranked by their potential impact on GPC adoption. The single most significant constraint on in-situ GPC use is heat-curing dependency in FA-rich systems; binary FA/GGBFS blends with 40–60% slag show the greatest promise for reliable ambient curing, but consistent performance across the precursor variability encountered in practice requires both chemical optimisation and robust adaptive characterisation protocols (Tahwia et al., 2024). An open-access, community-maintained multi-source experimental database for FA/GGBFS GPC, analogous to the CEB-FIP model code database for OPC concrete, with standardised data entry requirements covering precursor XRF data, mix proportions, curing protocol, and 28-day results; the largest published ML training datasets currently contain fewer than 1,500 data points, insufficient for robust generalisation (Kong et al., 2025; Golafshani et al., 2024). Longitudinal field monitoring programmes using non-destructive testing (NDT) methods (cover-meter surveys, half-cell potential mapping, ground-penetrating radar, and rebound hammer) are needed to validate laboratory-derived service-life predictions for carbonation and chloride ingress at the structural scale (Nodehi & Taghvaee, 2022; Wasim et al., 2021). The projected EU coal phase-out by 2030 demands proactive research into calcined clay, CDW glass, biomass silica, and geologically diverse volcanic materials to ensure precursor supply security for FA-dependent GPC production (Islam et al., 2025; Qin et al., 2022; Roychand et al., 2023). Finally, replacing chemically manufactured Na_2SiO_3 with waste-derived silicate activators, the highest-priority environmental intervention for reducing GPC's acidification potential and fossil resource depletion beyond the GWP metric, requires dedicated research into activator consistency, solubility, and reactivity across diverse waste silica sources (Fort et al., 2024; Passuello et al., 2017).

13. Conclusions

This review presents a synthesis of the current state of knowledge on FA/GGBFS-based geopolymer concrete, focusing on reaction chemistry, mix design, mechanical performance, durability, environmental sustainability, and engineering application. Five principal conclusions are drawn:

1. Binary FA/GGBFS GPC achieves 28-day compressive strengths of 45–85 MPa under ambient curing. GGBFS content, NaOH molarity (8–14 M), SS/SH ratio (1.5–2.5), and w/b ratio (0.35–0.40) are the four dominant governing variables, collectively accounting for over 85% of observed strength variability.
2. ML-assisted multi-objective optimisation identifies FA/GGBFS ≈ 1:3 as the balanced design point for ambient-cured structural GPC when strength, cost, and CO2 are optimised simultaneously.
3. GPC offers mechanistically well-understood durability advantages over OPC concrete in chemically aggressive environments (less strength loss in H2SO4, zero ettringite formation in FA-dominant formulations under Na2SO4 exposure, RCPT values below 2,000 C in binary FA/GGBFS systems, and greater than 90% strength retention at 800°C) in FA-dominant and binary FA/GGBFS systems.
4. LCA studies show CO_2 reductions of 35–65% versus OPC, with Na_2SiO_3 as the dominant remaining environmental burden. Multi-criterion LCA should replace single-indicator GWP as the standard.

5. The proposed GPC Performance Classification Matrix provides the first evidence-based five-tier specification framework linking precursor chemistry, gel type, strength grade, durability class, and application.
6. Barriers to adoption include absent harmonised standards, precursor variability, and limited long-term field data. Open-access databases and standardisation are the highest-leverage interventions requiring immediate action.

Declarations

Author Contributions Statement: Ibrahim Alameri: Writing- Original draft preparation; Salam R. Armoosh: Image preparation; F. E. Hanash: Supervision, Final Drafting. All authors reviewed the manuscript and approved it.

Ethical approvals:

Not Applicable.

Consent to participate:

Not Applicable.

Consent to publish:

Not applicable.

Competing interests:

The Authors have no conflicts of interest.

Clinical trial number

Not Applicable.

Funding:

None

Author Contribution

Ibrahim Alameri wrote the main manuscript text Salam R. Armoosh prepared figures and tables.F. E. Hanash reviewed the manuscript.

Acknowledgements:

None

Availability of data and materials:

Not applicable.

References

1. Adewuyi YG. Recent Advances in Fly-Ash-Based Geopolymers: Potential on the Utilization for Sustainable Environmental Remediation. ACS Omega. 2021;6(24):15532–42. https://doi.org/10.1021/acsomega.1c00662.
2. Afsoosbiria H, Machowska A. Development of Sustainable Concrete Using By-Products as a Green Material, and Potential Solutions for Sustainability in Mass Concrete. Construction—Comprehensive Rev Sustainability. 2025;17(22):9983. https://doi.org/10.3390/su17229983.
3. Ahmaruzzaman M. A review on the utilization of fly ash. Prog Energy Combust Sci. 2010;36(3):327–63. https://doi.org/10.1016/j.pecs.2009.11.003.
4. Aïtcin P-C. Cements of yesterday and today. Cem Concr Res. 2000;30(9):1349–59. https://doi.org/10.1016/S0008-8846(00)00365-3.
5. Al Khaffaf I, Hawileh RA, Sahoo S, Abdalla JA, Kim JH. Toward carbon- neutral construction: A review of zero-carbon concrete. J Building Eng. 2025;99:111578. https://doi.org/10.1016/j.jobe.2024.111578.
6. Alahmari TS, Abdalla TA, Rihan MAM. Review of Recent Developments Regarding the Durability Performance of Eco-Friendly Geopolymer Concrete. Buildings. 2023;13(12):3033. https://doi.org/10.3390/buildings13123033.
7. Almutairi AL, Tayeh BA, Adesina A, Isleem HF, Zeyad AM. Potential applications of geopolymer concrete in construction: A review. Case Stud Constr Mater. 2021;15:e00733. https://doi.org/10.1016/j.cscm.2021.e00733.
8. Amin M, Elsakhawy Y, Abu El-Hassan K, Abdelsalam BA. Behavior evaluation of sustainable high strength geopolymer concrete based on fly ash, metakaolin, and slag. Case Stud Constr Mater. 2022;16:e00976. https://doi.org/10.1016/j.cscm.2022.e00976.
9. Amran YHM, Alyousef R, Alabduljabbar H, El-Zeadani M. Clean production and properties of geopolymer concrete; A review. J Clean Prod. 2020;251:119679. https://doi.org/10.1016/j.jclepro.2019.119679.
10. Aslan S, Erkan İH. The Effects of Fly Ash, Blast Furnace Slag, and Limestone Powder on the Physical and Mechanical Properties of Geopolymer Mortar. Appl Sci. 2024;14(2):553. https://doi.org/10.3390/app14020553.
11. Bakharev T. Durability of geopolymer materials in sodium and magnesium sulfate solutions. Cem Concr Res. 2005;35(6):1233–46. https://doi.org/10.1016/j.cemconres.2004.09.002.
12. Berends CJ, De Boer B, Van De Wal RSW. Reconstructing the evolution of ice sheets, sea level, and atmospheric CO_2 during the past 3.6 million years. Clim Past. 2021;17(1):361–77. https://doi.org/10.5194/cp-17-361-2021.
13. Bernal SA, Provis JL, Walkley B, San Nicolas R, Gehman JD, Brice DG, Kilcullen AR, Duxson P, Van Deventer JSJ. Gel nanostructure in alkali-activated binders based on slag and fly ash, and effects of accelerated carbonation. Cem Concr Res. 2013;53:127–44. https://doi.org/10.1016/j.cemconres.2013.06.007.

14. Blissett RS, Rowson NA. A review of the multi-component utilisation of coal fly ash. Fuel. 2012;97:1–23. https://doi.org/10.1016/j.fuel.2012.03.024.
15. Boutkhil H, Fellak S, Alehyen S, Bari A, Fidan H. Physico-chemical properties and durability of a fly-ash-based geopolymer. Open Chem. 2024;22(1):20240048. https://doi.org/10.1515/chem-2024-0048.
16. Brekke S, O'Born R. (2025). Life Cycle Assessment of Geopolymer Concrete Made with Tailings from Ilmenite Mining. In M. Kioumarsi & B. Shafei, editors, *The 1st International Conference on Net-Zero Built Environment* (Vol. 237, pp. 821–829). Springer Nature Switzerland. https://doi.org/10.1007/978-3-031-69626-8_69
17. Castel A, Foster SJ. Bond strength between blended slag and Class F fly ash geopolymer concrete with steel reinforcement. Cem Concr Res. 2015;72:48–53. https://doi.org/10.1016/j.cemconres.2015.02.016.
18. Cheng D, Reiner DM, Yang F, Cui C, Meng J, Shan Y, Liu Y, Tao S, Guan D. Projecting future carbon emissions from cement production in developing countries. Nat Commun. 2023;14(1):8213. https://doi.org/10.1038/s41467-023-43660-x.
19. Cong P, Du R, Gao H, Chen Z. Comparison and assessment of carbon dioxide emissions between alkali-activated materials and OPC cement concrete. J Traffic Transp Eng (English Edition). 2024;11(5):918–38. https://doi.org/10.1016/j.jtte.2023.07.011.
20. Da J, Zhang YG, Li G, Meng X, Ji J. Low CO2 levels of the entire Pleistocene epoch. Nat Commun. 2019;10(1):4342. https://doi.org/10.1038/s41467-019-12357-5.
21. Davidovits J. Geopolymers: Inorganic polymeric new materials. J Therm Anal. 1991;37(8):1633–56. https://doi.org/10.1007/BF01912193.
22. Davidovits J. Geopolymer: Chemistry and applications. Institut Géopolymère; 2008.
23. Deb PS, Nath P, Sarker PK. (2014). The effects of ground granulated blast-furnace slag blending with fly ash and activator content on the workability and strength properties of geopolymer concrete cured at ambient temperature. *Materials & Design (1980–2015)*, *62*, 32–39. https://doi.org/10.1016/j.matdes.2014.05.001
24. Degefu DM, Berardi U. Effect of Na/Al and curing moisture conditions on sodium aluminosilicate hydrate (N–A–S–H) geopolymers' hydric properties. Constr Build Mater. 2024;425:135985. https://doi.org/10.1016/j.conbuildmat.2024.135985.
25. Duxson P, Fernández-Jiménez A, Provis JL, Lukey GC, Palomo A, Van Deventer JSJ. Geopolymer technology: The current state of the art. J Mater Sci. 2007;42(9):2917–33. https://doi.org/10.1007/s10853-006-0637-z.
26. El Fadili H, Ait-Khouia Y, Ouffa N, Taha Y, Moukannaa S, Benzaazoua M. Comprehensive review on alkaline dissolution of aluminosilicates and its role in the mechanisms and properties of geopolymers and alkali-activated materials. Case Stud Constr Mater. 2025;23:e05330. https://doi.org/10.1016/j.cscm.2025.e05330.
27. Emarah DA. Multivariate predictive modeling of compressive strength in ground granulated blast furnace slag/fly ash-based alkali-activated concrete. Clean Eng Technol. 2025;27:101021. https://doi.org/10.1016/j.clet.2025.101021.
28. Farooq F, Jin X, Javed F, Akbar M, Izhar Shah A, Aslam M, F., Alyousef R. Geopolymer concrete as sustainable material: A state of the art review. Constr Build Mater. 2021;306:124762. https://doi.org/10.1016/j.conbuildmat.2021.124762.

29. Fernández-Jiménez A, Palomo A. Composition and microstructure of alkali activated fly ash binder: Effect of the activator. Cem Concr Res. 2005;35(10):1984–92. https://doi.org/10.1016/j.cemconres.2005.03.003.
30. Fořt J, Mildner M, Černý R. Consequences of omitting some important factors in the environmental analyses of commercial sodium silicate/sodium hydroxide use for alkaline activation in the light of comparison with cement-based composites. Sci Total Environ. 2024;928:172324. https://doi.org/10.1016/j.scitotenv.2024.172324.
31. Freire AL, José HJ, Moreira RDFPM. Potential applications for geopolymers in carbon capture and storage. Int J Greenhouse Gas Control. 2022;118:103687. https://doi.org/10.1016/j.ijggc.2022.103687.
32. Giergiczny Z. Fly ash and slag. Cem Concr Res. 2019;124:105826. https://doi.org/10.1016/j.cemconres.2019.105826.
33. Gluth GJG, Arbi K, Bernal SA, Bondar D, Castel A, Chithiraputhiran S, Dehghan A, Dombrowski-Daube K, Dubey A, Ducman V, Peterson K, Pipilikaki P, Valcke SLA, Ye G, Zuo Y, Provis JL. RILEM TC 247-DTA round robin test: Carbonation and chloride penetration testing of alkali-activated concretes. Mater Struct. 2020;53(1):21. https://doi.org/10.1617/s11527-020-1449-3.
34. Golafshani E, Khodadadi N, Ngo T, Nanni A, Behnood A. Modelling the compressive strength of geopolymer recycled aggregate concrete using ensemble machine learning. Adv Eng Softw. 2024;191:103611. https://doi.org/10.1016/j.advengsoft.2024.103611.
35. Hamsashree, Pandit P, Prashanth S, Katpady DN. Durability of alkali-activated fly ash-slag concrete- state of art. Innovative Infrastructure Solutions. 2024;9(6):222. https://doi.org/10.1007/s41062-024-01530-5.
36. Hardjito D, Wallah SE, Sumajouw DMJ, Rangan BV. On the Development of Fly Ash-Based Geopolymer Concrete. ACI Mater J. 2004;101(6). https://doi.org/10.14359/13485.
37. Hönisch B, Royer DL, Breecker DO, Polissar PJ, Bowen GJ, Henehan MJ, Cui Y, Steinthorsdottir M, McElwain JC, Kohn MJ, Pearson A, Phelps SR, Uno KT, Ridgwell A, Anagnostou E, Austermann J, Badger MPS, Barclay RS, Bijl PK, Zhang L. Toward a Cenozoic history of atmospheric CO2. Science. 2023;382(6675):eadi5177. https://doi.org/10.1126/science.adi5177.
38. Hu Y, Tang Z, Li W, Li Y, Tam VWY. Physical-mechanical properties of fly ash/GGBFS geopolymer composites with recycled aggregates. Constr Build Mater. 2019;226:139–51. https://doi.org/10.1016/j.conbuildmat.2019.07.211.
39. Hussein SS, Fawzi NM. Influence of Using Various Percentages of Slag on Mechanical Properties of Fly Ash-based Geopolymer Concrete. J Eng. 2021;27(10):50–67. https://doi.org/10.31026/j.eng.2021.10.04.
40. IPCC, editor. Climate Change 2022 - Mitigation of Climate Change: Working Group III Contribution to the Sixth Assessment Report of the Intergovernmental Panel on Climate Change. 1st ed. Cambridge University Press; 2023. https://doi.org/10.1017/9781009157926.
41. Islam MT, Kafle B, Al-Ameri R. Natural Clay in Geopolymer Concrete: A Sustainable Alternative Pozzolanic Material for Future Green Construction—A. Compr Rev Sustainability. 2025;17(22):10180. https://doi.org/10.3390/su172210180.
42. Ismail I, Bernal SA, Provis JL, Hamdan S, Van Deventer JSJ. Microstructural changes in alkali activated fly ash/slag geopolymers with sulfate exposure. Mater Struct. 2013;46(3):361–73. https://doi.org/10.1617/s11527-012-9906-2.
43. Khasawneh MA. Geopolymer concrete in construction projects: A review. Discover Civil Eng. 2025;2(1):124. https://doi.org/10.1007/s44290-025-00281-1.

44. Kolade AS, Ikotun BD, Oyejobi DO. A Review of the Chemistry, Waste Utilization, Mix Design and Performance Evaluation of Geopolymer Concrete. Iran J Sci Technol Trans Civil Eng. 2025;49(6):5421–54. https://doi.org/10.1007/s40996-025-01801-w.
45. Kong X, Zhang M, Kai M, Zhao Y, Ren J, Gu Z. Optimization of Fly ash-slag based geopolymer strength, cost, and carbon emissions using CNN-based RSM and NSGA-III. Constr Build Mater. 2025;501:144380. https://doi.org/10.1016/j.conbuildmat.2025.144380.
46. Kumar S, Kumar R, Bandopadhyay A, Alex TC, Ravi Kumar B, Das SK, Mehrotra SP. Mechanical activation of granulated blast furnace slag and its effect on the properties and structure of portland slag cement. Cem Concr Compos. 2008;30(8):679–85. https://doi.org/10.1016/j.cemconcomp.2008.05.005.
47. Lee NK, Lee HK. Setting and mechanical properties of alkali-activated fly ash/slag concrete manufactured at room temperature. Constr Build Mater. 2013;47:1201–9. https://doi.org/10.1016/j.conbuildmat.2013.05.107.
48. Lokesha EB, Aruna M, Reddy SK. Durability characteristics of geopolymer concrete produced using gold ore tailings along with recycled coarse aggregates. Sci Rep. 2025;15(1):12051. https://doi.org/10.1038/s41598-025-97056-6.
49. Lothenbach B, Scrivener K, Hooton RD. Supplementary cementitious materials. Cem Concr Res. 2011;41(12):1244–56. https://doi.org/10.1016/j.cemconres.2010.12.001.
50. Luo Y, Klima KM, Brouwers HJH, Yu Q. Effects of ladle slag on Class F fly ash geopolymer: Reaction mechanism and high temperature behavior. Cem Concr Compos. 2022;129:104468. https://doi.org/10.1016/j.cemconcomp.2022.104468.
51. Martínez A, Miller SA. Life cycle assessment and production cost of geopolymer concrete: A meta-analysis. Resour Conserv Recycl. 2025;215:108018. https://doi.org/10.1016/j.resconrec.2024.108018.
52. Marvila MT, Azevedo ARGD, Vieira CMF. Reaction mechanisms of alkali-activated materials. Revista IBRACON de Estruturas e Materiais. 2021;14(3):e14309. https://doi.org/10.1590/s1983-41952021000300009.
53. Matsimbe J, Dinka M, Olukanni D, Musonda I. Geopolymer: A Systematic Review of Methodologies. Materials. 2022;15(19):6852. https://doi.org/10.3390/ma15196852.
54. Mehta A, Siddique R. Sulfuric acid resistance of fly ash based geopolymer concrete. Constr Build Mater. 2017;146:136–43. https://doi.org/10.1016/j.conbuildmat.2017.04.077.
55. Mehta A, Siddique R, Ozbakkaloglu T, Ahmed Shaikh U, F., Belarbi R. Fly ash and ground granulated blast furnace slag-based alkali-activated concrete: Mechanical, transport and microstructural properties. Constr Build Mater. 2020;257:119548. https://doi.org/10.1016/j.conbuildmat.2020.119548.
56. Meshram RB, Kumar S. Comparative life cycle assessment (LCA) of geopolymer cement manufacturing with Portland cement in Indian context. Int J Environ Sci Technol. 2022;19(6):4791–802. https://doi.org/10.1007/s13762-021-03336-9.
57. Meyer C. The greening of the concrete industry. Cem Concr Compos. 2009;31(8):601–5. https://doi.org/10.1016/j.cemconcomp.2008.12.010.
58. Myers RJ, Bernal SA, San Nicolas R, Provis JL. Generalized Structural Description of Calcium–Sodium Aluminosilicate Hydrate Gels: The Cross-Linked Substituted Tobermorite Model. Langmuir. 2013;29(17):5294–306. https://doi.org/10.1021/la4000473.

59. Naaman AE, Reinhardt HW. Proposed classification of HPFRC composites based on their tensile response. Mater Struct. 2007;39(5):547–55. https://doi.org/10.1617/s11527-006-9103-2.
60. Naresh T, Mallik M, Rao SV, Sameer M, Dora RK, Kumar VVP, Prasad NSS. Synergistic effects of rice husk ash and neutral silicate activator on rheology and strength of ambient-cured self-compacting geopolymer concrete. Discover Concrete Cem. 2026;2(1):6. https://doi.org/10.1007/s44416-026-00048-6.
61. Nath P, Sarker PK. Effect of GGBFS on setting, workability and early strength properties of fly ash geopolymer concrete cured in ambient condition. Constr Build Mater. 2014;66:163–71. https://doi.org/10.1016/j.conbuildmat.2014.05.080.
62. Neville AM. Properties of concrete. 5th ed. Pearson; 2011.
63. Nodehi M, Taghvaee VM. Alkali-Activated Materials and Geopolymer: A Review of Common Precursors and Activators Addressing Circular Economy. Circular Econ Sustain. 2022;2(1):165–96. https://doi.org/10.1007/s43615-021-00029-w.
64. Page MJ, McKenzie JE, Bossuyt PM, Boutron I, Hoffmann TC, Mulrow CD, Shamseer L, Tetzlaff JM, Akl EA, Brennan SE, Chou R, Glanville J, Grimshaw JM, Hróbjartsson A, Lalu MM, Li T, Loder EW, Mayo-Wilson E, McDonald S, Moher D. The PRISMA 2020 statement: An updated guideline for reporting systematic reviews. BMJ. 2021;n71. https://doi.org/10.1136/bmj.n71.
65. Palomo A, Grutzeck MW, Blanco MT. Alkali-activated fly ashes. Cem Concr Res. 1999;29(8):1323–9. https://doi.org/10.1016/S0008-8846(98)00243-9.
66. Paruthi S, Rahman I, Khan AH, Sharma N, Alyaseen A. Strength, durability, and economic analysis of GGBS-based geopolymer concrete with silica fume under harsh conditions. Sci Rep. 2024;14(1):31572. https://doi.org/10.1038/s41598-024-77801-z.
67. Passuello A, Rodríguez ED, Hirt E, Longhi M, Bernal SA, Provis JL, Kirchheim AP. Evaluation of the potential improvement in the environmental footprint of geopolymers using waste-derived activators. J Clean Prod. 2017;166:680–9. https://doi.org/10.1016/j.jclepro.2017.08.007.
68. Pearson PN, Palmer MR. Atmospheric carbon dioxide concentrations over the past 60 million years. Nature. 2000;406(6797):695–9. https://doi.org/10.1038/35021000.
69. Polusani S, Ram VV, Rao MVS. Life Cycle Assessment of geopolymer concrete using Flyash and Slag for sustainable infrastructure. Innovative Infrastructure Solutions. 2025;10(7):270. https://doi.org/10.1007/s41062-025-02084-w.
70. Provis JL. Alkali-activated materials. Cem Concr Res. 2018;114:40–8. https://doi.org/10.1016/j.cemconres.2017.02.009.
71. Provis JL, Palomo A, Shi C. Advances in understanding alkali-activated materials. Cem Concr Res. 2015;78:110–25. https://doi.org/10.1016/j.cemconres.2015.04.013.
72. Provis JL, Van Deventer JSJ, editors. (2014). *Alkali Activated Materials: State-of-the-Art Report, RILEM TC 224-AAM* (Vol. 13). Springer Netherlands. https://doi.org/10.1007/978-94-007-7672-2
73. Puertas F, Martínez-Ramírez S, Alonso S, Vázquez T. Alkali-activated fly ash/slag cements. Cem Concr Res. 2000;30(10):1625–32. https://doi.org/10.1016/S0008-8846(00)00298-2.
74. Puligilla S, Mondal P. Role of slag in microstructural development and hardening of fly ash-slag geopolymer. Cem Concr Res. 2013;43:70–80. https://doi.org/10.1016/j.cemconres.2012.10.004.

75. Qin Y, Qu C, Ma C, Zhou L. One-Part Alkali-Activated Materials: State of the Art and Perspectives. Polymers. 2022;14(22):5046. https://doi.org/10.3390/polym14225046.
76. Rae JWB, Zhang YG, Liu X, Foster GL, Stoll HM, Whiteford RDM. Atmospheric CO_2 over the Past 66 Million Years from Marine Archives. Annu Rev Earth Planet Sci. 2021;49(1):609–41. https://doi.org/10.1146/annurev-earth-082420-063026.
77. Rahimpour H, Esmaeili J. Characterization, mechanical strength, rheological properties and life cycle assessment of fully recycled concrete through geopolymer technology. Sci Rep. 2025;15(1):9424. https://doi.org/10.1038/s41598-025-92307-y.
78. Rashad AM. A comprehensive overview about the influence of different admixtures and additives on the properties of alkali-activated fly ash. Mater Design. 2014;53:1005–25. https://doi.org/10.1016/j.matdes.2013.07.074.
79. Rossi L, De Lima M, Sun L, Dehn Y, Provis F, Ye J, G., De Schutter G. Future perspectives for alkali-activated materials: From existing standards to structural applications. RILEM Tech Lett. 2023;7:159–77. https://doi.org/10.21809/rilemtechlett.2022.160.
80. Roychand R, Li J, Kilmartin-Lynch S, Saberian M, Zhu J, Youssf O, Ngo T. Carbon sequestration from waste and carbon dioxide mineralisation in concrete – A stronger, sustainable and eco-friendly solution to support circular economy. Constr Build Mater. 2023;379:131221. https://doi.org/10.1016/j.conbuildmat.2023.131221.
81. Samantasinghar S, Singh SP. Fresh and Hardened Properties of Fly Ash–Slag Blended Geopolymer Paste and Mortar. Int J Concrete Struct Mater. 2019;13(1):47. https://doi.org/10.1186/s40069-019-0360-1.
82. Scrivener KL, John VM, Gartner EM. Eco-efficient cements: Potential economically viable solutions for a low-CO2 cement-based materials industry. Cem Concr Res. 2018;114:2–26. https://doi.org/10.1016/j.cemconres.2018.03.015.
83. Shahmansouri AA, Nematzadeh M, Behnood A. Mechanical properties of GGBFS-based geopolymer concrete incorporating natural zeolite and silica fume with an optimum design using response surface method. J Building Eng. 2021;36:102138. https://doi.org/10.1016/j.jobe.2020.102138.
84. Shehata N, Mohamed OA, Sayed ET, Abdelkareem MA, Olabi AG. Geopolymer concrete as green building materials: Recent applications, sustainable development and circular economy potentials. Sci Total Environ. 2022;836:155577. https://doi.org/10.1016/j.scitotenv.2022.155577.
85. Shi X, Zhang C, Liang Y, Luo J, Wang X, Feng Y, Li Y, Wang Q, Abomohra AE-F. Life Cycle Assessment and Impact Correlation Analysis of Fly Ash Geopolymer Concrete. Materials. 2021;14(23):7375. https://doi.org/10.3390/ma14237375.
86. Van Sindhunata JSJ, Lukey GC, Xu H. Effect of Curing Temperature and Silicate Concentration on Fly-Ash-Based Geopolymerization. Ind Eng Chem Res. 2006;45(10):3559–68. https://doi.org/10.1021/ie051251p.
87. Singh J, Singh SP. Geopolymerization of solid waste of non-ferrous metallurgy – A review. J Environ Manage. 2019;251:109571. https://doi.org/10.1016/j.jenvman.2019.109571.
88. Singh PK, Rajhans P. Effect of surface treatment and mixing approach on the durability performance of recycled aggregate geopolymer concrete against aggressive environment. J Building Eng. 2025;101:111867. https://doi.org/10.1016/j.jobe.2025.111867.
89. Singh RP, Vanapalli KR, Cheela VRS, Peddireddy SR, Sharma HB, Mohanty B. Fly ash, GGBS, and silica fume based geopolymer concrete with recycled aggregates: Properties and environmental impacts. Constr Build

Mater. 2023;378:131168. https://doi.org/10.1016/j.conbuildmat.2023.131168.

90. Taher MJ, Saffar A, Motloq DM, Khalil RF, W. I., Abed EH. (2024). *A review on hardened properties, durability and microstructure of slag geopolymer composite*. 060003. https://doi.org/10.1063/5.0211048
91. Tahwia AM, Aldulaimi DS, Abdellatief M, Youssf O. Physical, Mechanical and Durability Properties of Eco-Friendly Engineered Geopolymer Composites. Infrastructures. 2024;9(11):191. https://doi.org/10.3390/infrastructures9110191.
92. Turner LK, Collins FG. Carbon dioxide equivalent (CO2-e) emissions: A comparison between geopolymer and OPC cement concrete. Constr Build Mater. 2013;43:125–30. https://doi.org/10.1016/j.conbuildmat.2013.01.023.
93. Tushar Q, Bhuiyan MA, Abunada Z, Lemckert C, Giustozzi F. Carbon Footprint and Uncertainties of Geopolymer Concrete Production: A Comprehensive Life Cycle Assessment (LCA). C. 2025;11(3):55. https://doi.org/10.3390/c11030055.
94. Van Roijen E, Sethares K, Kendall A, Miller SA. The climate benefits from cement carbonation are being overestimated. Nat Commun. 2024;15(1):4848. https://doi.org/10.1038/s41467-024-48965-z.
95. Verma M, Dev N. Sodium hydroxide effect on the mechanical properties of flyash-slag based geopolymer concrete. Struct Concrete. 2021;22(S1). https://doi.org/10.1002/suco.202000068.
96. Wan H, Yuan L, Zhang Y. Insight Into the Leaching of Sodium Alumino-Silicate Hydrate (N-A-S-H) Gel: A Molecular Dynamics Study. Front Mater. 2020;7:56. https://doi.org/10.3389/fmats.2020.00056.
97. Wang Z, Chen S, Zheng X, Huang X, Fu T, Feng C, Yu D, Zhang H. Mechanism of Activation and Mechanical Properties of Alkali-Activated Material Derived from GGBFS/FA Activated by Carbide Slag. Materials. 2026;19(7):1313. https://doi.org/10.3390/ma19071313.
98. Wasim M, Ngo TD, Law D. A state-of-the-art review on the durability of geopolymer concrete for sustainable structures and infrastructure. Constr Build Mater. 2021;291:123381. https://doi.org/10.1016/j.conbuildmat.2021.123381.
99. Wong LS. Durability Performance of Geopolymer Concrete: A Review. Polymers. 2022;14(5):868. https://doi.org/10.3390/polym14050868.
100. Wudil YS, Al-Fakih A, Al-Osta MA, Gondal MA. Intelligent optimization for modeling carbon dioxide footprint in fly ash geopolymer concrete: A novel approach for minimizing CO2 emissions. J Environ Chem Eng. 2024;12(1):111835. https://doi.org/10.1016/j.jece.2023.111835.
101. Xiao L, Zhang C, Zhang H, Jiang Z. Internal Curing Effects of Slag on Properties and Microstructure of Ambient-Cured Fly Ash-Based Geopolymer Mortar. Buildings. 2024;14(12):3846. https://doi.org/10.3390/buildings14123846.
102. Xu H, Van Deventer JSJ. The geopolymerisation of alumino-silicate minerals. Int J Miner Process. 2000;59(3):247–66. https://doi.org/10.1016/S0301-7516(99)00074-5.
103. Yao ZT, Ji XS, Sarker PK, Tang JH, Ge LQ, Xia MS, Xi YQ. A comprehensive review on the applications of coal fly ash. Earth Sci Rev. 2015;141:105–21. https://doi.org/10.1016/j.earscirev.2014.11.016.
104. Yazıcı N, Karagöl F. Assessing the effects of Na_2 SO_4 and NaCl on the properties of geopolymer concrete subjected to elevated temperatures. Struct Concrete. 2024;25(5):3841–65. https://doi.org/10.1002/suco.202300985.

105. Zhang P, Gao Z, Wang J, Guo J, Hu S, Ling Y. Properties of fresh and hardened fly ash/slag based geopolymer concrete: A review. J Clean Prod. 2020;270:122389. https://doi.org/10.1016/j.jclepro.2020.122389.

106. Zhao C, Li J, Zhu Z, Guo Q, Wu X, Wang Z, Zhao R. Research on the Carbonation Resistance and Carbonation Depth Prediction Model of Fly Ash- and Slag-Based Geopolymer Concrete. KSCE J Civ Eng. 2024;28(7):2802–17. https://doi.org/10.1007/s12205-024-1767-z.

Figures

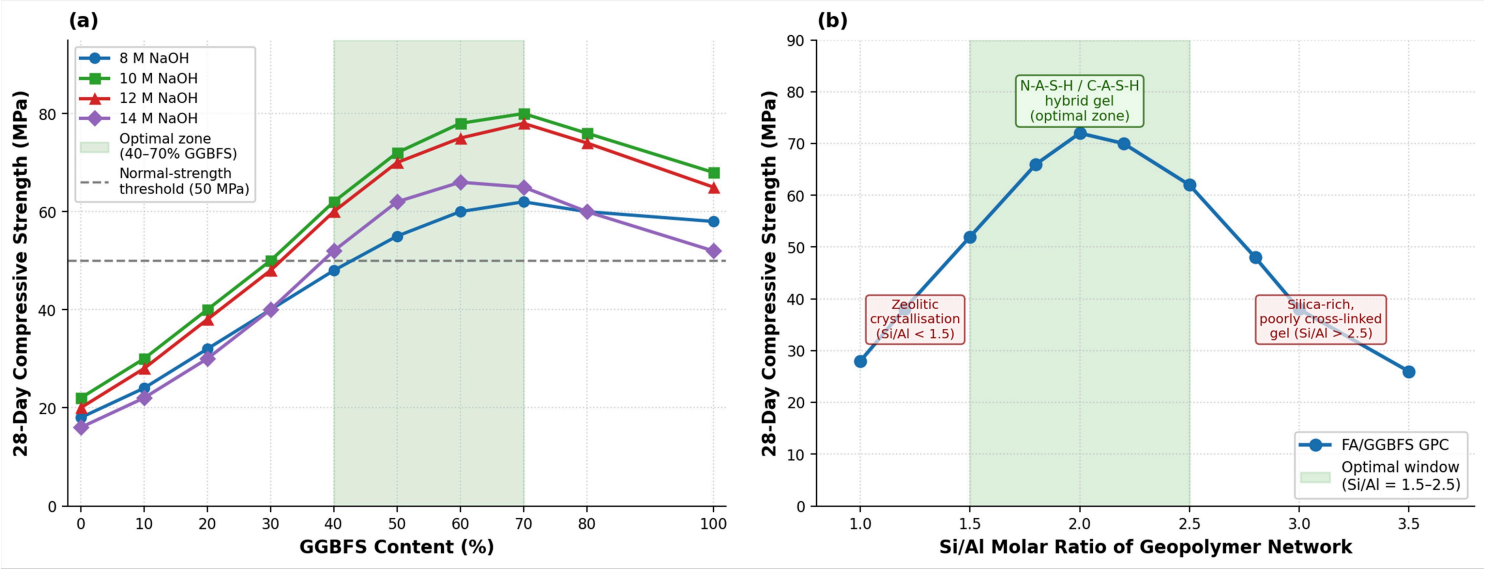


Figure 1

(a28-day compressive strength vs. GGBFS content (Hussein & Fawzi, 2021; Nath & Sarker, 2014; Samantasinghar & Singh, 2019; Zhao et al., 2024) (b) Compressive strength vs. Si/Al molar ratio (Duxson et al., 2007; Zhang et al., 2020).

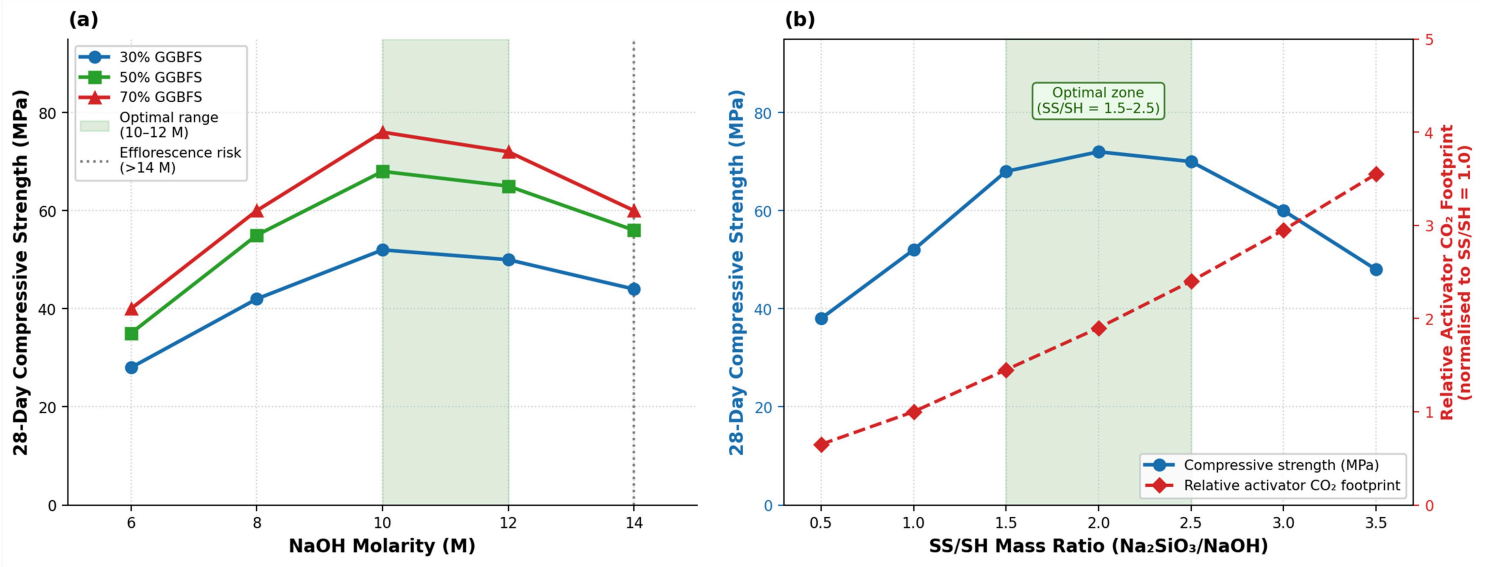


Figure 2

(a) 28-day compressive strength vs. NaOH molarity (Aslan & Erkan, 2024; Hussein & Fawzi, 2021; Samantasinghar & Singh, 2019) *(b) Compressive strength vs. SS/SH mass ratio, with relative activator CO_2 footprint* (Fořt et al., 2024; Hussein & Fawzi, 2021; Zhang et al., 2020)

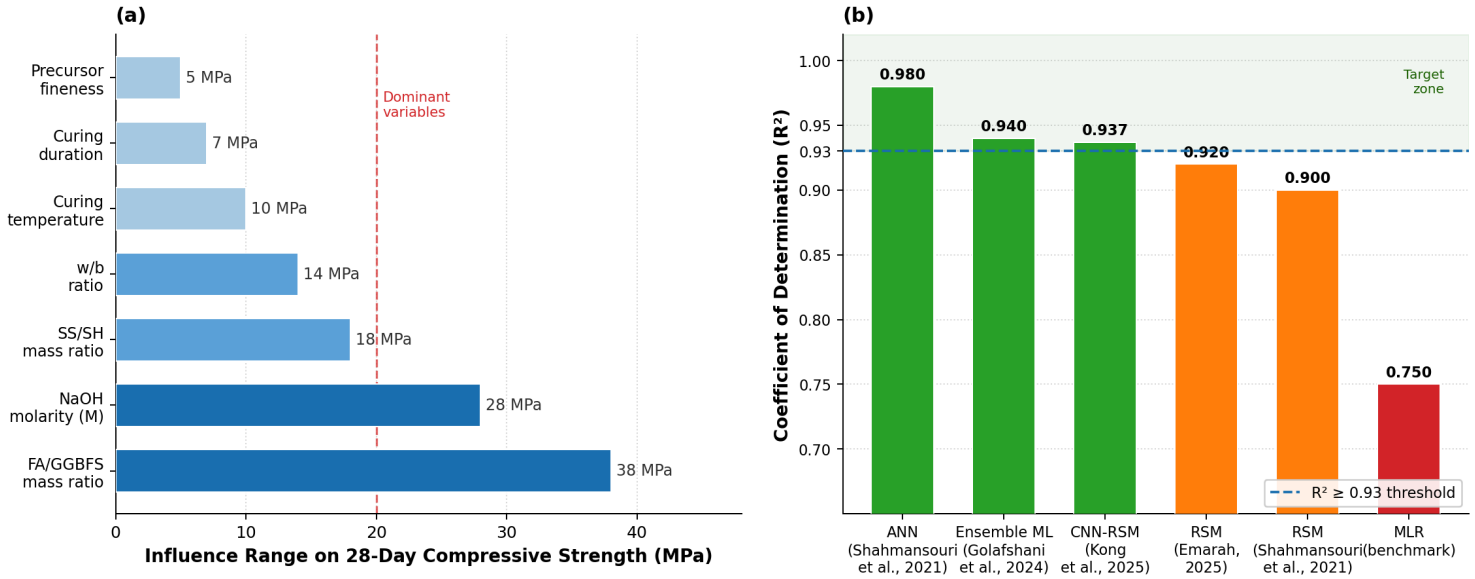


Figure 3

(a) Sensitivity analysis of seven mix design parameters on 28-day compressive strength (Kong et al., 2025; Emarah, 2025; Golafshani et al., 2024). (b) Comparison of R² values of predictive models for GPC compressive strength (Shahmansouri et al., 2021; Golafshani et al., 2024; Kong et al., 2025; Emarah, 2025).

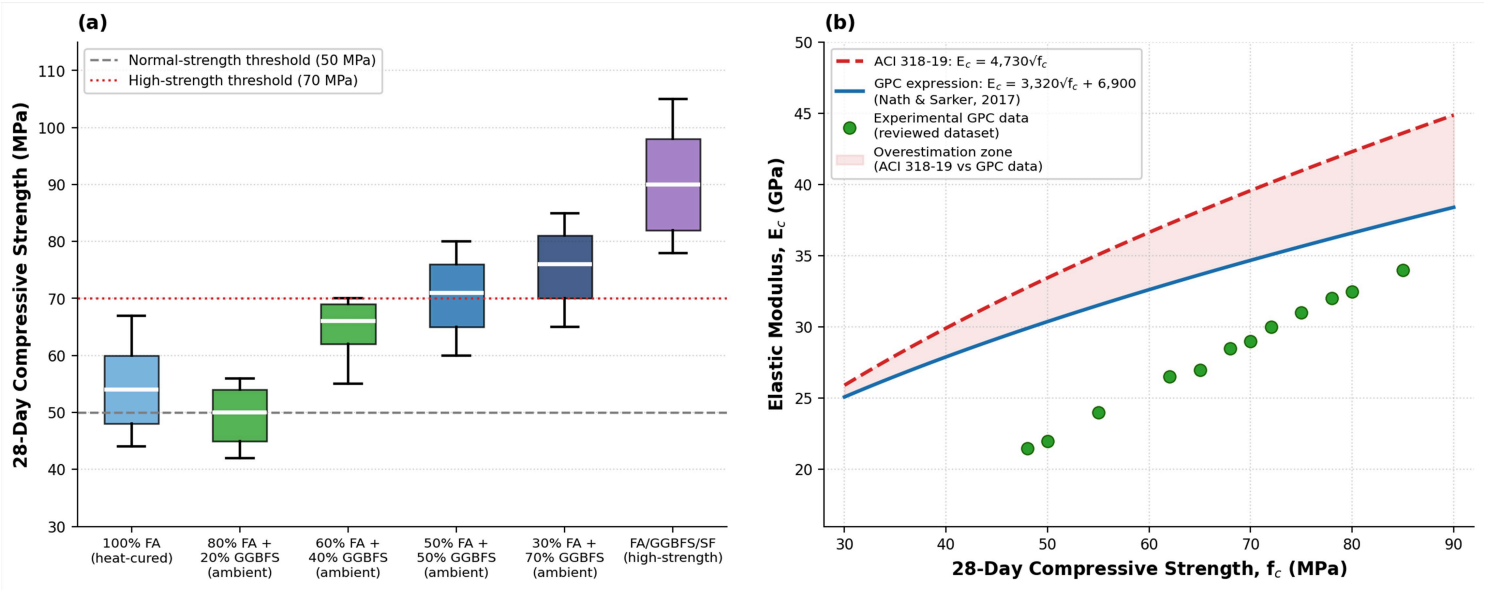


Figure 4

(a) Distribution of 28-day compressive strength (Zhang et al., 2020; Hardjito et al., 2004; Samantasinghar & Singh, 2019; Deb et al., 2014; Lee & Lee, 2013; Kong et al., 2025; (Hussein & Fawzi, 2021)*; Verma & Dev, 2021, 2022; Mehta & Siddique, 2020; Zhao et al., 2024;* (Amin et al., 2022)*; Paruthi et al., 2024). (b) Elastic modulus vs. compressive strength for binary FA/GGBFS GPC.*

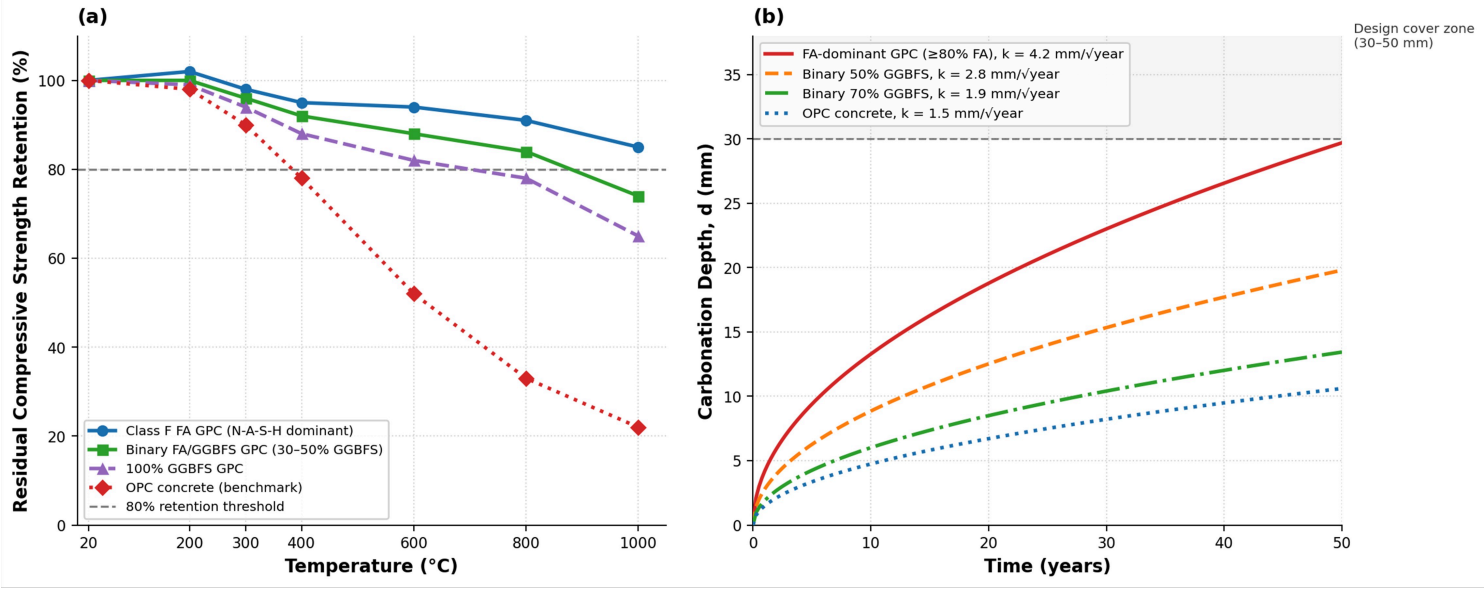


Figure 5

(a) Residual compressive strength retention after exposure from ambient to 1000°C ((Khasawneh, 2025)*; Alahmari et al., 2023; Taher et al., 2024). (b) Predicted carbonation depth over 50 years using diffusion-controlled kinetics (Zhao et al., 2024; Bernal et al., 2013).*

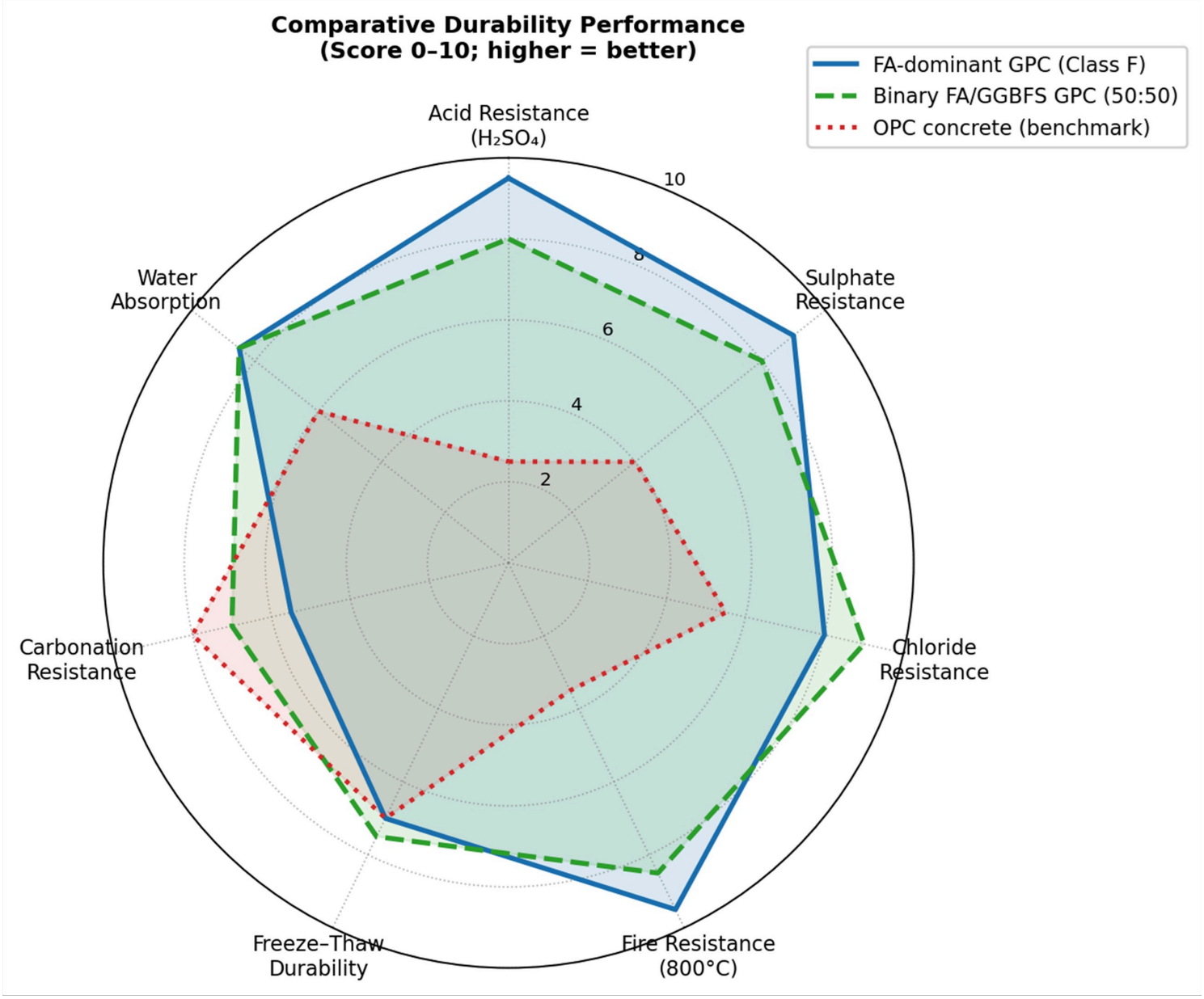


Figure 6

Durability of FA-dominant, FA/GGBFS (50:50), and OPC concrete across seven mechanisms (Mehta & Siddique, 2017; Bakharev, 2005; Ismail et al., 2013; Wong, 2022; (Khasawneh, 2025)*; Alahmari et al., 2023; Zhao et al., 2024;* (Hamsashree et al., 2024)*; Samantasinghar & Singh, 2019).*

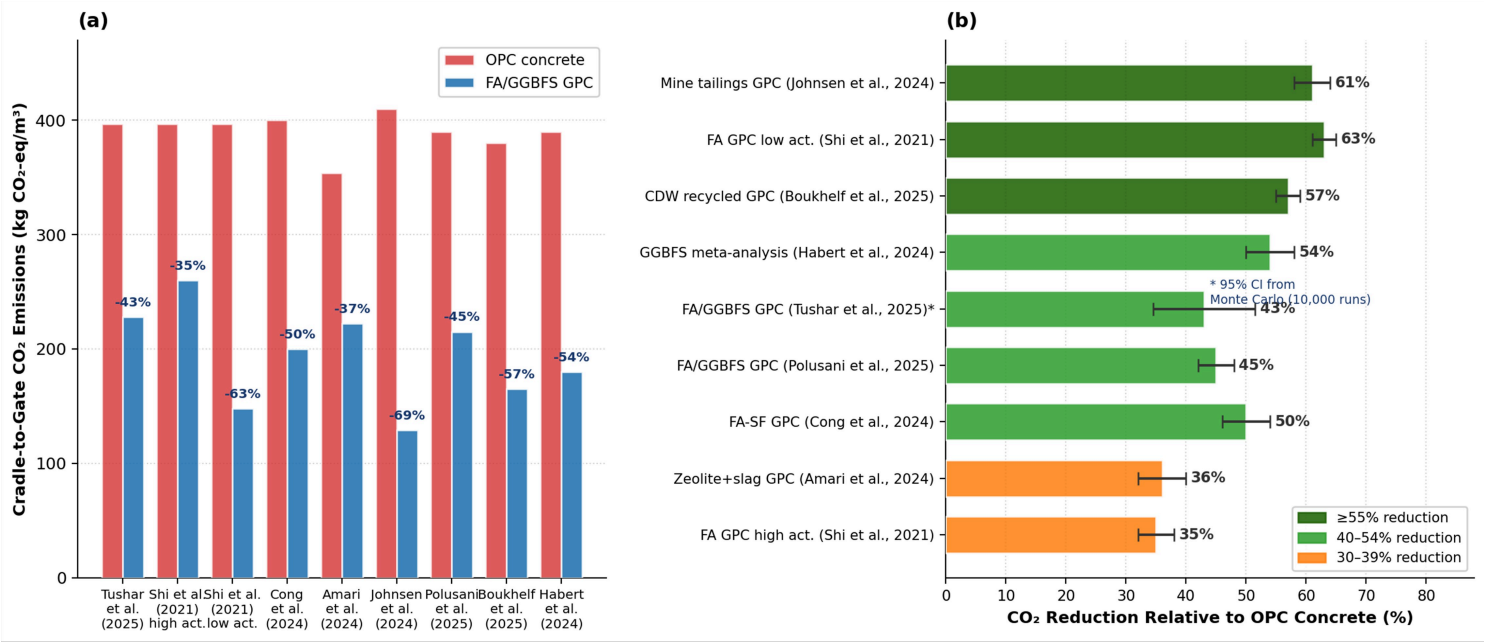


Figure 7

(a) Cradle-to-gate CO_2 emissions of FA/GGBFS GPC vs. OPC (Tushar et al., 2025; Shi et al., 2021; Cong et al., 2024; Amari et al., 2024; (Brekke & O'Born, 2025)*; Polusani et al., 2025; Rahimpour & Esmaeili, 2025). (b) CO_2 reduction relative to OPC baseline.*